STATE RESEARCH CENTER OF RUSSIA
INSTITUTE FOR HIGH ENERGY PHYSICS
RU-142284, Protvino, Moscow Region, Russia

NuMI–B–652
June 30, 2000

Advanced Conceptual Design of the NuMI Hadron Beam Absorber Core

(Task A Report of the Accord between FNAL and IHEP)

A.Abramov, S.Filippov, P.Galkin, N.Galyaev, V.Garkusha,
A.Kharlamov, E.Lomakin, F.Novoskoltsev,
A.Ryabov, V.Zarucheisky

Contents

1 Introduction

The design goal of the NuMI hadron absorber core (the actively cooled region in the beam stop at the end of the decay pipe) [1] is to absorb the most part of the beam energy and to transfer it to the water cooling loop. The remaining energy should be absorbed in steel shielding around and behind the absorber core.

Besides of the regular operation mode, when a properly steered primary proton beam interacts with the production target, the material, length and transverse dimensions of an absorber core should be defined also by the incidental operation mode (the emergency), when a primary proton beam does not interact in the target and during a relatively short period of time directly strikes the absorber core.

An interim information on the absorber core design is collected at the Absorber Studies web site[1]. This information includes results of energy deposition calculations in a core material, descriptions of various conceptions of the absorber core, as well as results of temperature and stress calculations for two variants of an absorber core and for steel shielding blocks around and behind the absorber core.

The present Report, which was prepared after the approval of core configuration and construction techniques by the NuMI WBS 1.1.4 sub-project manager[2], describes the variant of core design with cooling pipe clamped between two aluminum slabs (labeled as variant "A" in our preliminary notes). Fulfilling the recommendation of the DOE 11/99 NuMI Review, Report gives also results of calculations of stresses induced by the proposed single turn extracted primary beam. Cooling of the steel shielding outside the core and a general conception of replacing of failure core modules are included in the consideration.

[1] http://www-numi.fnal.gov:8875/monthly_reports/secure/core.html.
[2] A.Wehmann's e-mail from June 13, 2000.

2 Energy Deposition in the Absorber

2.1 Outline

This Section gives results of energy deposition calculations in the absorber for three configurations of the PH2 focusing system. Some estimations were also made for the ME beam with the Hadronic Hose. The energy deposition were calculated using the MARS [2] computer code for the 120 GeV resonant extracted primary beam with 4×10^{13} protons per spill. The total energy of a primary beam is equal to 768 kJ or 404 kW in terms of an average power taking into account the 1.9 s repetition period.

Distributions of a resonant extracted proton beam in the target are given in Figure 2.1a. These distributions were obtained by the M.C. simulation of a beam transport from the electrostatic deflector entrance to the NuMI target and then were directly used in MARS runs. For the missteered primary proton beam, which does not interact with a target, corresponding distributions in front of the absorber are given in Figure 2.1b.

Energy deposition calculations were made for two possible operation modes (regular and emergency) with binning required for subsequent temperature and stress calculations. Taking into account results of preliminary calculations of an energy deposition in the absorber core, an aluminum was chosen as a suitable core material. The transverse dimensions (1.32×1.32 m^2) and the length (2.4 m) of an aluminum core result from:

- possible positions of the proton beam axis in front of the absorber in case when a missteered primary proton beam does not interact with a target ($R \simeq 0.42$ m)[3];
- dimensions of 52"$\times$52"$\times$26" steel blocks[4], which may be used as steel shielding around and behind the absorber core.

Besides the aluminum core, the MARS model for energy deposition calculations includes also the 1.32 m length steel block located behind the aluminum core and the 1.32 m thick rectangular steel shielding surrounding the central part of the absorber.

[3]This value is determined by baffle collimators which protect horn necks from direct heating by a primary proton beam.

[4]These recycled low-radioactivity steel blocks are mentioned on page 4 of A.Wehmann's paper "Update of NuMI Absorber Conceptual Design" from October 8, 1999.

2.2 Energy Deposition in the Absorber for the ME Beam

2.2.1 Energy Distribution in Front of the Absorber

Only ~1/6 of a total energy of a primary beam reaches the absorber in the regular operation mode (see Table 2.1), while remaining energy is dissipated in shielding located in the target enclosure and along the decay pipe. The main part of an energy (~80%) is brought to the absorber by non-interacting primary protons, including primary protons passing the target in tails of their x and y distributions. Radial distributions of energy densities in front of the absorber are given in Figure 2.2 and show, that about 80% of a total beam energy falls on the absorber core.

Total energy in a beam		121.2 kJ
Energy of primary protons		99.7 kJ
Energy of secondaries:	π, p	16.1 kJ
	n, e, γ	5.4 kJ
Average beam power		64 kW

Table 2.1: Beam parameters in front of the absorber for the ME beam in the regular operation mode.

These radial distributions, as well as energy spectra in all radial bins were used for detail description of an energy flux distribution in front of the absorber, which allows to start subsequent MARS runs immediately before an absorber. Such an approach to calculations of an energy deposition in the absorber proves to be very helpful from the point of view of an accuracy of calculations versus CPU time consumption. Moreover, it saves a lot of time when calculations of an energy deposition should be made for some different variants of an absorber design.

In the emergency, when the missteered primary proton beam does not interact with a target, distributions of an energy in front of the absorber coincide with distributions of a primary proton beam (Figure 2.1b).

2.2.2 Energy Deposition in the Regular Operation Mode

Cumulative and differential longitudinal distributions of the average power deposited in the absorber are shown in Figures 2.3 and 2.4 respectively. The total average power deposited in the absorber is equal to 57 kW and is distributed in different parts of the absorber as it is shown in Table 2.2.

Part of the absorber	$0 \leq Z < 2.4$ m	$2.4 \leq Z < 3.7$ m
Core and subsequent steel	41.0 (Al)	5.7 (Fe)
Surrounding steel shielding	10.2	0.14

Table 2.2: The average power (kW) deposited in the absorber for the ME beam. The total deposited power is equal to 57 kW.

The most heated part of the absorber core (7.8 kW per one 0.3 m length aluminum slab) is located at $Z = 0.6 \div 1.2$ m. Transverse distributions of an energy deposition density in this cross-section of the core, as well as in the upstream part of the steel block located behind the core (4.1 kW in the first 0.3 m length part of the steel block) are given in Figure 2.5.

The analysis of a power deposition in steel shielding around the central part of the absorber shows, that approximately 90% from 10.2 kW is deposited along the first meter of shielding. This power is essentially deposited in 2, 4, 6 and 8 zones of an absorber cross-section (see sketch given in Figure 2.3), while zones 3, 5, 7 and 9, located apart the decay pipe, are practically not heated by an incident beam. Transverse distributions of an average power deposited in each from 2, 4, 6 and 8 zones (2.55 kW in total with 0.84 kW in the first 0.3 m bin) are given in Figure 2.6.

2.2.3 Energy Deposition in the Emergency

The distribution of an energy deposition density along the proton beam axis in case when the missteered primary proton beam directly strikes the absorber are shown in Figure 2.7. Transverse distributions of an energy deposition density in the cross-section, where the energy deposition density on the beam axis reaches its maximum value and in the upstream part of a steel block behind the core are given in Figure 2.8.

The energy deposition density reaches its maximum values of 21 J/cm^3 per one beam spill in the aluminum absorber core ($Z \simeq 0.75$ m)[5] and 10 J/cm^3 in the upstream part of the steel block behind the core. Simple estimations of corresponding temperature jumps (with a specific heat C_p taken at the temperature 297°K) give 8.5°C in the aluminum and 2.8°C in the subsequent steel block.

[5] This value is approximately 2 times larger than that given in A.Wehmann's report "Energy Deposition in the Absorber Core" from October 19, 1999, what could be explained by a difference in primary proton beam parameters in front of the absorber for these two MARS runs.

2.3 Energy Deposition in the Absorber for other Configurations of the PH2 Focusing System

2.3.1 LE and HE Beams

Described above results of energy deposition calculations in the absorber were obtained for the ME beam configuration of the PH2 focusing system. Two other beam configurations (LE and HE) differ from the ME one by an energy of a neutrino beam in the detector and, correspondingly, by an energy of secondaries focused by the toroidal magnetic field in two horns.

Non-interacting with a target primary protons pass to the absorber through field free holes in the horn necks even for the HE beam configuration with the second horn located 40 m downstream the first one. Because in all cases the target is two interaction lengths, the contribution of non-interacting with a target primary protons to the energy flux in front of the absorber is constant ($\sim$100 kJ) for all beam configurations.

Otherwise, the flux of charged secondary hadrons, which undergo the action of horns, varies from $\sim$5 kJ for the LE beam up to 44 kJ for the HE beam (16 kJ for the considered above ME beam). As a result, the total energy in front of the absorber for the HE beam reaches the value of 147 kJ, what is factor 1.2 higher than that for the ME beam. This leads to approximately the same increase of the average power deposited in the absorber as it is shown in Table 2.3. For the LE beam the total energy in front of the absorber and, correspondingly, the average deposited power are somewhat smaller than those for the ME beam.

Part of the absorber	$0 \leq Z < 2.4$ m	$2.4 \leq Z < 3.7$ m
Core and subsequent steel	45.6 (Al)	6.2 (Fe)
Surrounding steel shielding	14.3	0.24

Table 2.3: The average power (kW) deposited in the absorber for the HE beam. The total deposited power is equal to 66 kW.

So far as the baffle protection system is thus designed to protect the horn necks from direct heating by a primary proton beam independently of three possible positions of the second horn, the energy deposition in the absorber in the emergency is the same for all beam configurations (see 2.2.3).

2.3.2 ME Beam with the Hadronic Hose (Preliminary Results)

Given below preliminary results of MARS calculations show the significant decrease of an energy deposition in the absorber for the ME beam configuration with addition of the Hadronic Hose [3] (the 1.0 mm radius aluminum wire with the current of 1 kA along the decay pipe axis).

In the regular operation mode the total energy brought by the beam to the absorber is equal to ~48 kJ instead of 121 kJ for the ME beam configuration without the Hadronic Hose. This decrease is determined by two main changes in the energy flux in front of the absorber:

- a factor 4.4 decrease of the energy brought by primary protons, which intensively interact with a wire material;
- a factor 1.2 increase of the energy brought by charged secondary hadrons and n, e, γ component of the flux.

As a result, the average power deposited in the absorber (~22 kW) is a factor of 2.6 less compared to the ME beam configuration without the Hadronic Hose (see 2.2.2). The energy deposition density in the wire material reaches the value of ~2.5 J/cm^3 in the first 20 m part of the wire.

In the emergency with a primary proton beam passing the target 5 mm aside and parallel to the beamline axis, only ~5 kJ of an energy reaches the face of the absorber, while the maximum energy deposition density in the wire increases up to ~52 J/cm^3.

2.4 Summary

- The maximal average power is deposited in the absorber for the HE beam configuration (66 kW), while for the highest priority LE and ME beam configurations of the PH2 focusing system the average deposited power is about 57 kW.
- As follows from preliminary results for the ME beam, the use of the Hadronic Hose significantly decrease a heat load to the absorber.
- The minimal possible heat load to the absorber is expected (not still calculated) for the LE beam with addition of the beam plug, which intercepts the most of non-interacted primary protons and high energy secondaries directed to the absorber.

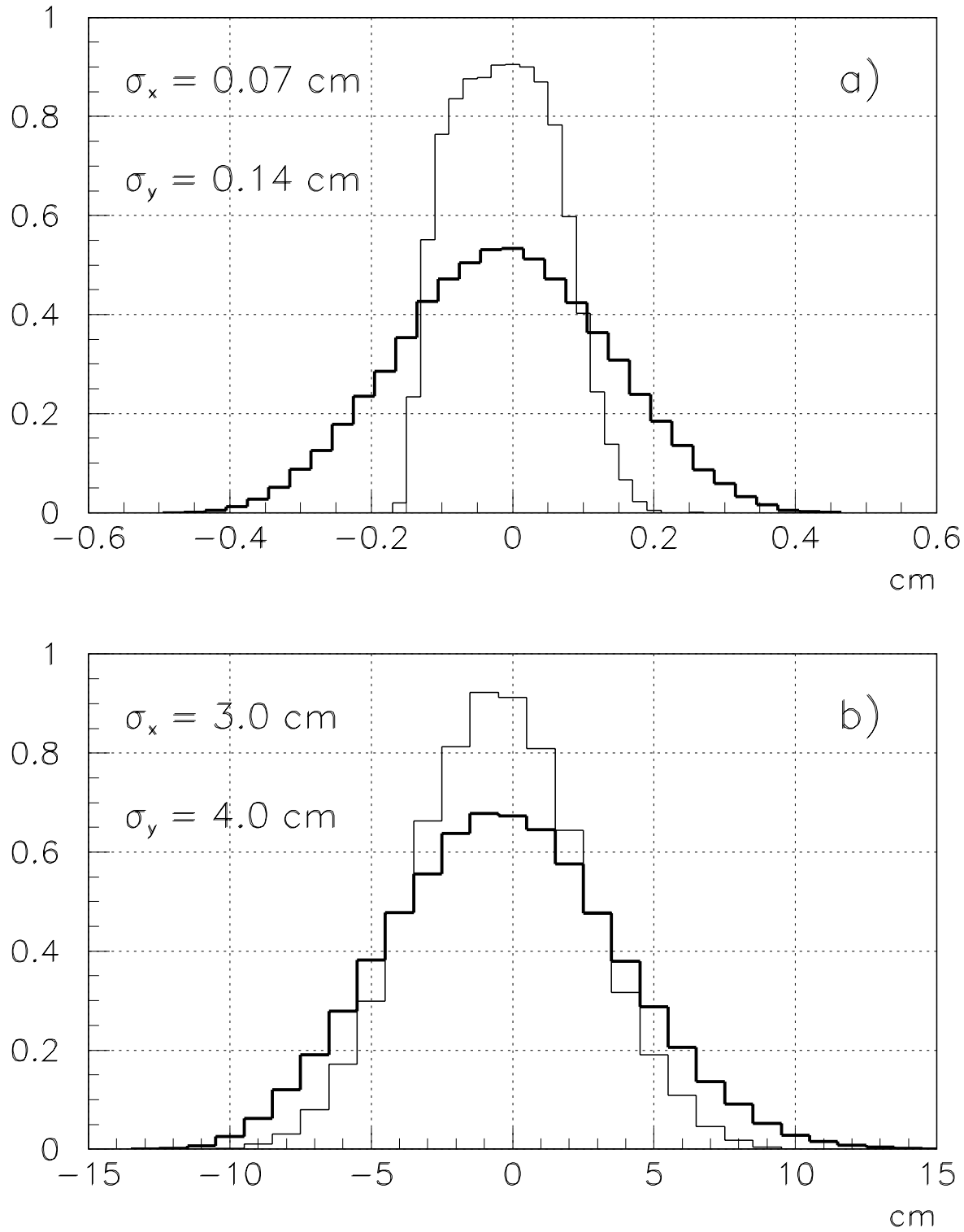

Figure 2.1: Distributions of a primary proton beam in the target (a) and in front of the absorber (b).

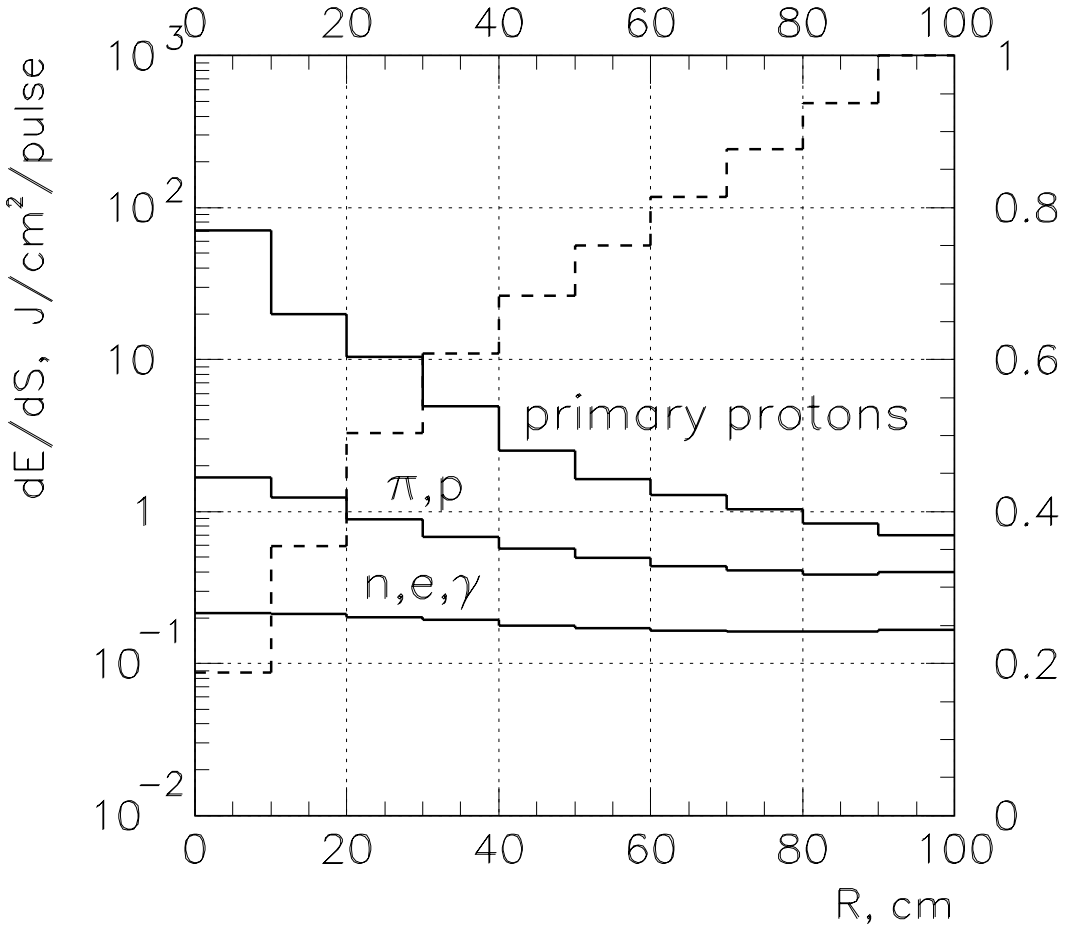

Figure 2.2: Radial distributions of beam energy densities in front of the absorber. Dash line gives cumulative radial distribution of the energy, normalized to the total beam energy (121 kJ) before the absorber.

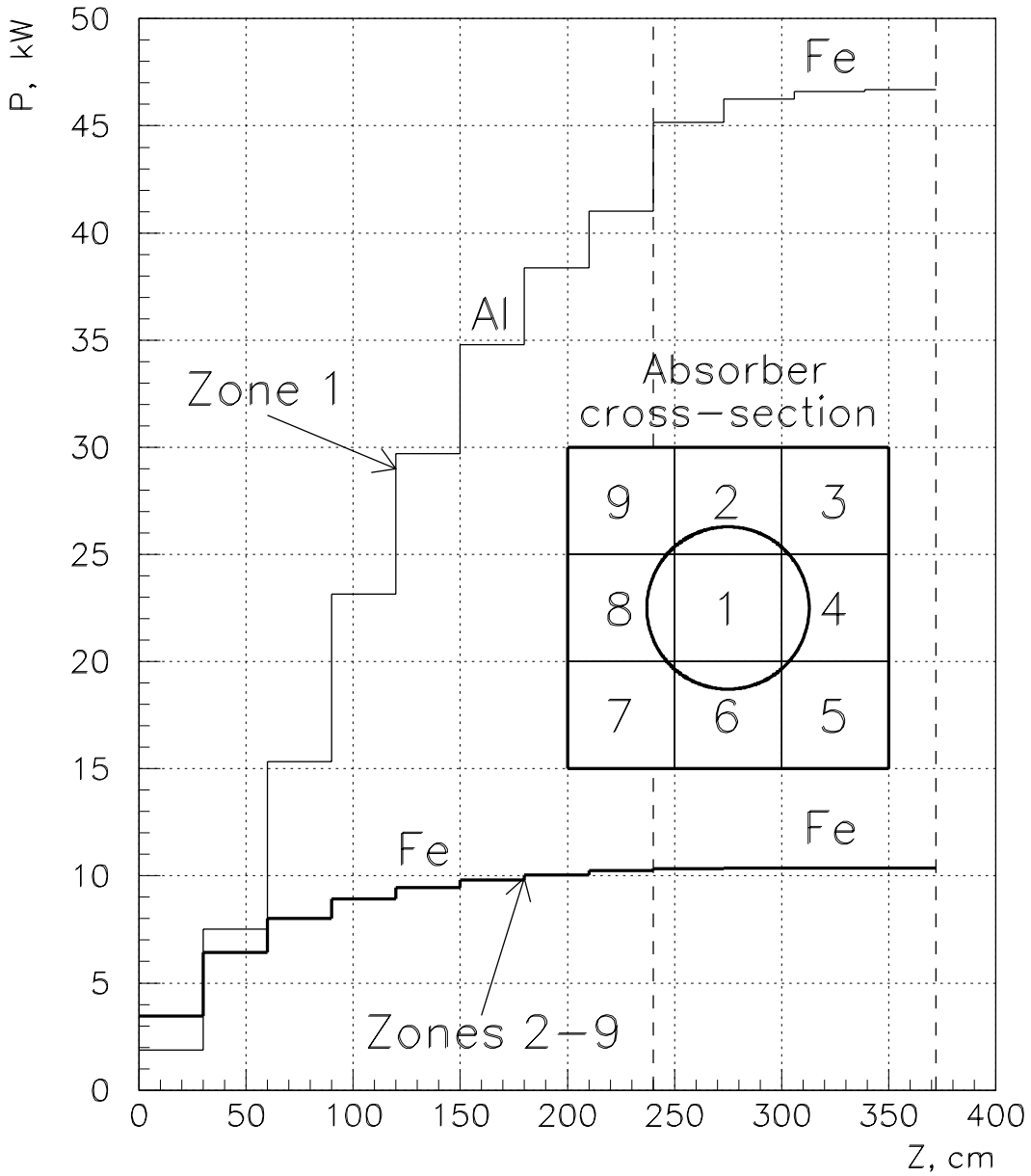

Figure 2.3: Cumulative longitudinal distributions of the average power deposited in the central part of the absorber with transverse sizes 1.32×1.32 m^2 (zone 1) and in 1.32 m thick steel shielding around the central part of the absorber (zones $2 \div 9$). The circle on the sketch of an absorber cross-section shows the size of the decay pipe.

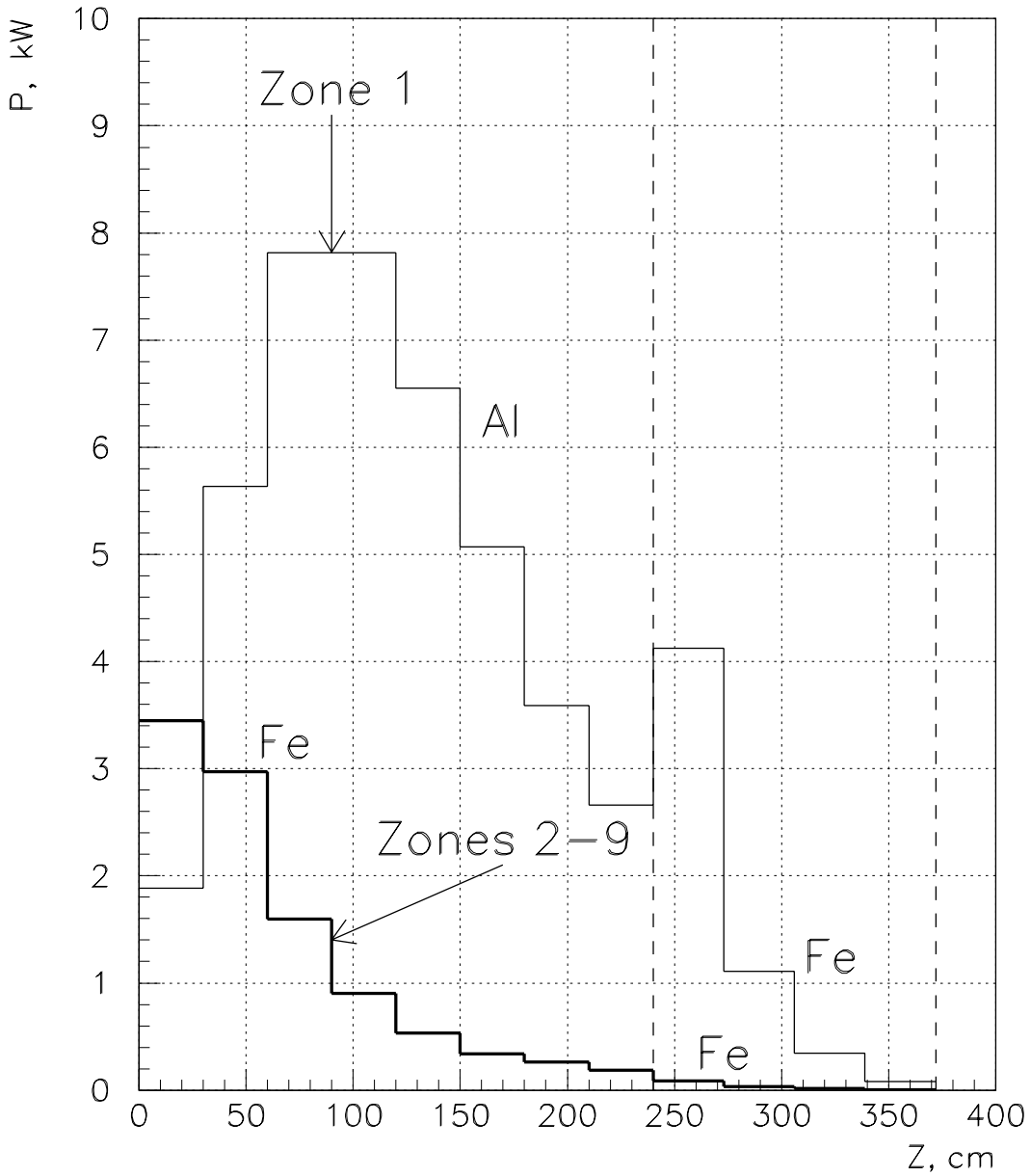

Figure 2.4: Longitudinal distributions of the average power deposited in the central part of the absorber with transverse sizes 1.32×1.32 m^2 (zone 1) and in 1.32 m thick steel shielding around the central part of the absorber (zones $2 \div 9$). See also the sketch of an absorber cross-section given in Figure 2.3.

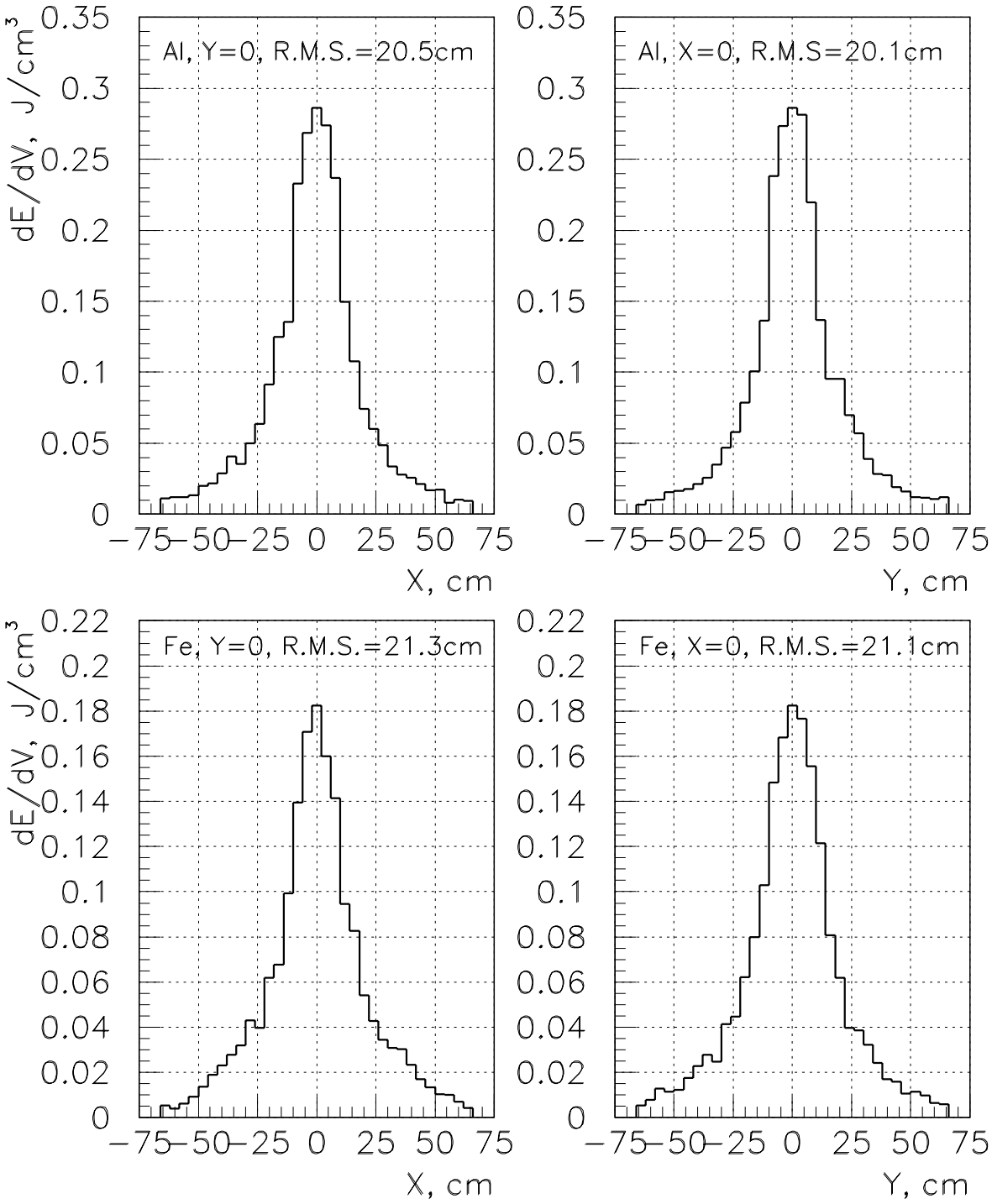

Figure 2.5: Transverse distributions of an energy deposition density for the most heated cross-section of an aluminum core at Z=0.8–0.9 m (top) and for the upstream part of a steel block behind the core at Z=2.4–2.5 m (bottom).

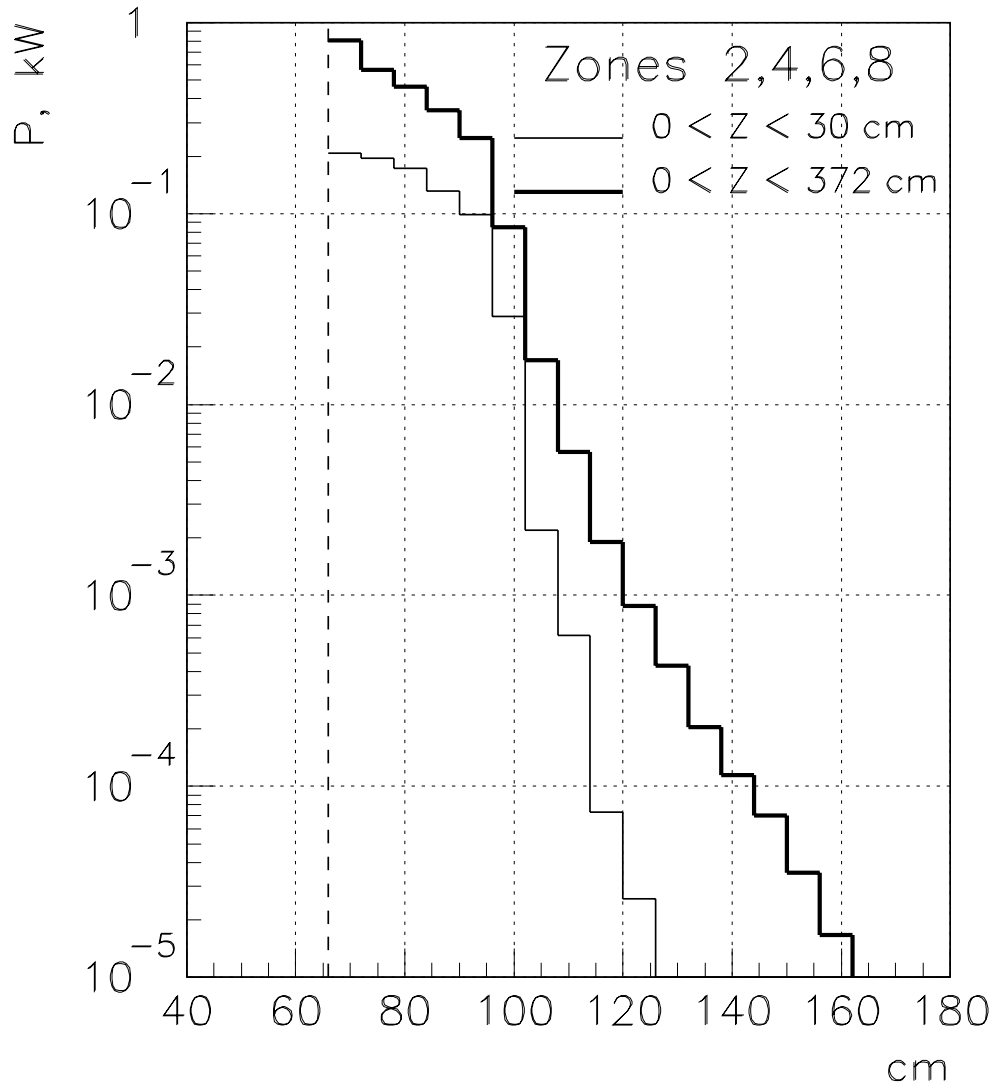

Figure 2.6: Transverse distributions of an average power deposited in one zone of the absorber cross-section. The sketch of an absorber cross-section is given in Figure 2.3.

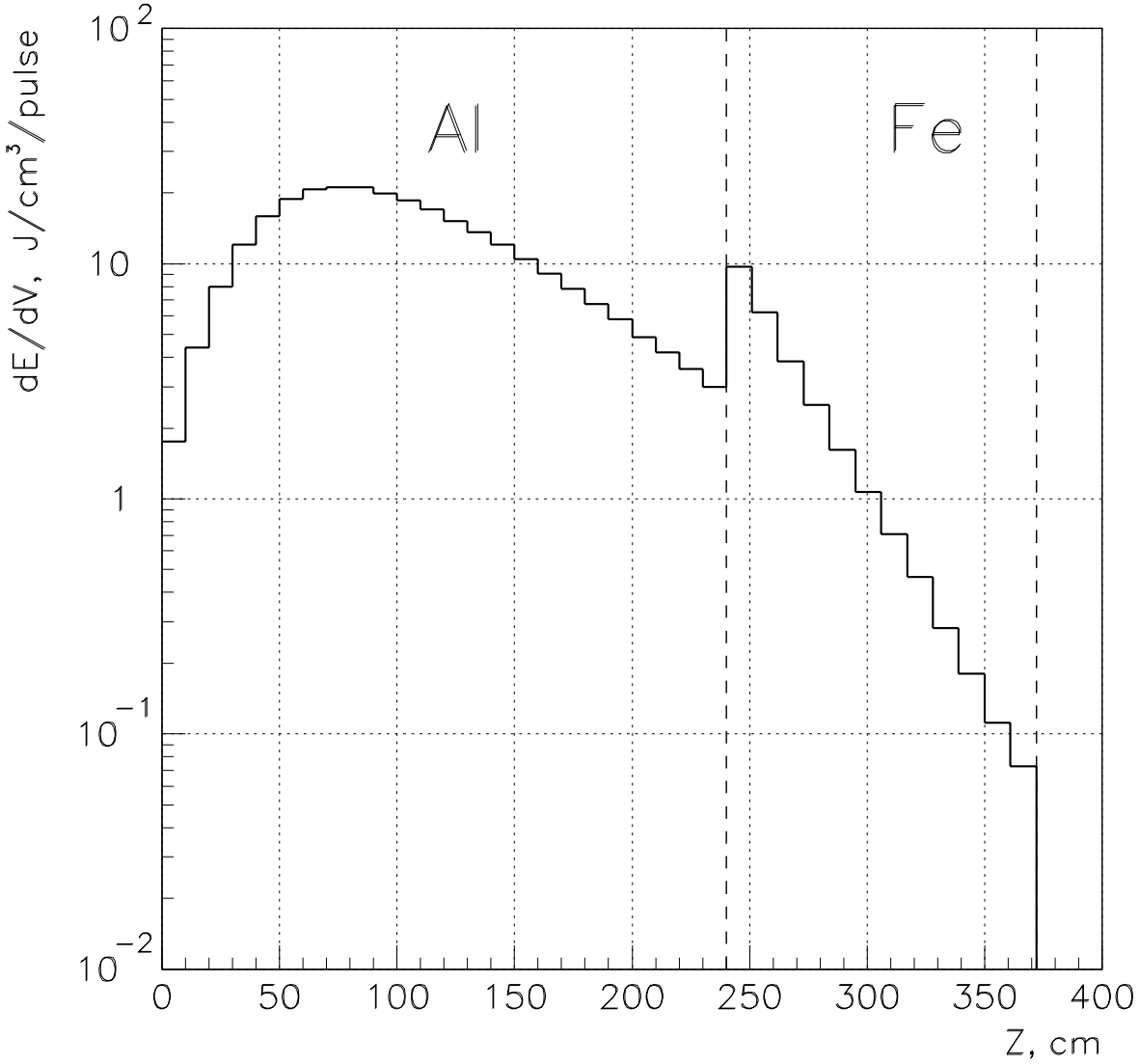

Figure 2.7: The distribution of an energy deposition density along the proton beam axis in case of the direct strike of the absorber by missteered proton beam.

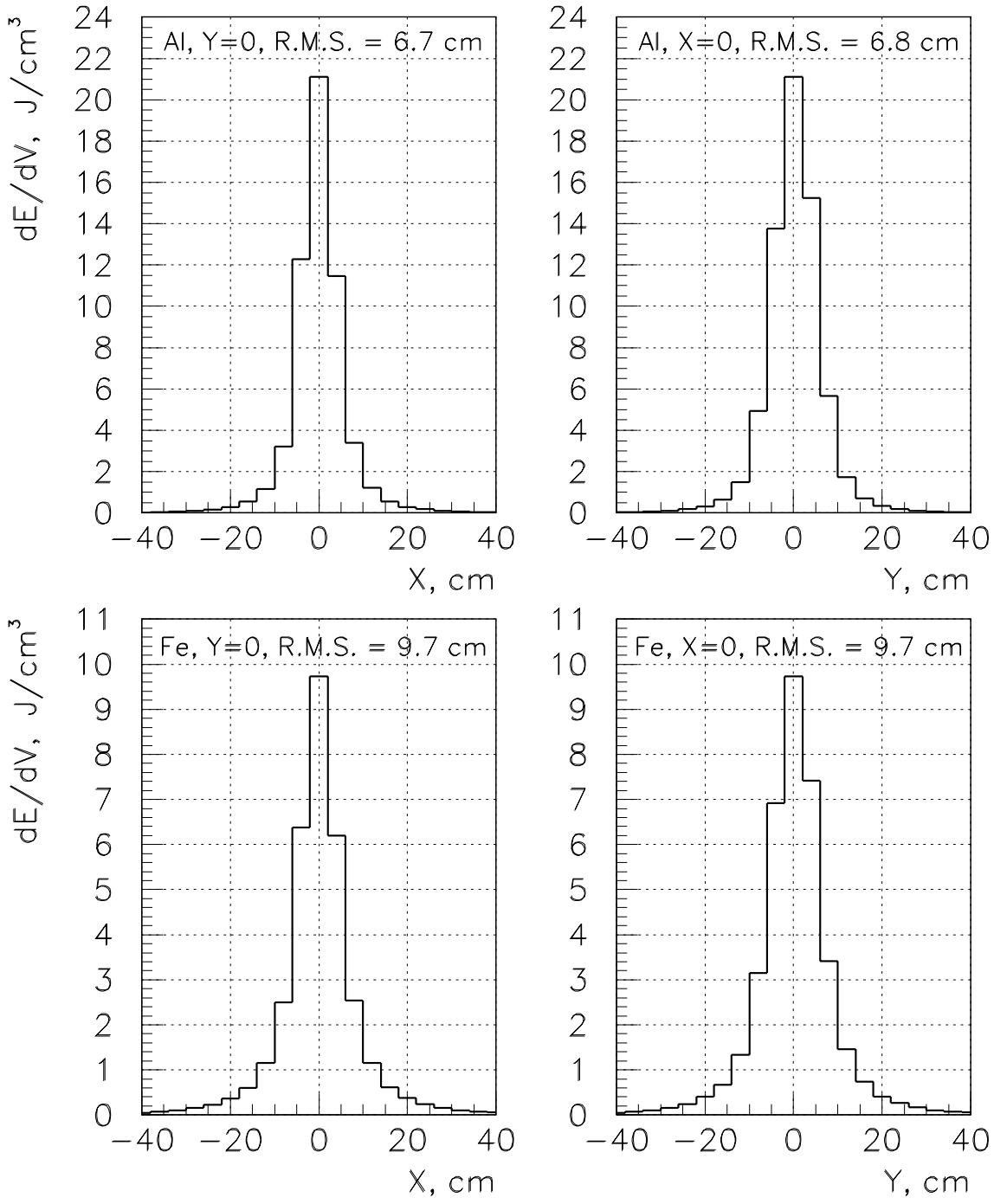

Figure 2.8: Transverse distributions of an energy deposition density in case of the direct strike of the absorber by missteered proton beam for the most heated cross-section of an aluminum core at Z=0.8–0.9 m (top) and for the upstream part of a steel block behind the core at Z=2.4–2.5 m (bottom).

3 Conceptual Design of the Absorber Core

3.1 General Description of the Absorber Core Design

The proposed design of an absorber core has a module structure (Figure 3.1) and is based on the following reasons:

- the Absorber Cavern will be constructed without overhead crane;
- the weight of each assembly unit should not exceed 10 tons;
- the water cooling system of an absorber core should be closed and very robust in order to minimize the risk of a water leakage;
- the design should reserve the possibility of making any necessary repairs or replaces of a failure module.

The transverse dimensions of the absorber core module (1.32×1.32 m^2) coincide with dimensions of mentioned above steel shielding blocks ($52" \times 52" \times 26"$). The thickness (the length along the beam) of the core module is chosen equal to $\sim$0.3 m, thus the total weight of an aluminum core module with an attached steel slab is about 6 tons (see Section 6). The absorber core consists of 8 separately cooled modules.

A cooling water passes through the 16.5 mm diameter hole in the 38.1×27.9 mm^2 aluminum pipe (buss), which is bent in the easier direction and pressed between two 0.15 m thick aluminum slabs. The necessary pressure ($\sim$3 MPa) is provided with help of 21 steel bolts with the diameter of 20 mm. Cooling pipes are connected outside the shielding to the general manifold of a water cooling system. The flow rate and the temperature of a water should be monitored during operation at both inlet and outlet of each parallel cooling line, as well as the temperature of each slab.

Because of an absence of any bolted or welded connections in a water cooling system of the core module, the risk of water leakage in the high radioactive area inside the absorber is practically excludes. At the same time, the proposed design of an absorber core module allows to have a second cooling line, which could be used in case of a failure of the first cooling line.

Some engineering problems of the proposed absorber core design are considered below after discussions of results of temperature and stress calculations.

3.2 Results of Temperature and Stress Calculations

Calculations of temperature and stresses in an aluminum core module were made with help of the ANSYS, solving the three-dimensional task of the heat transfer to a cooling water at the following boundary conditions:

- the temperature of a cooling water is equal to 37°C;
- the film coefficient is taken 8.5 kW/m^2·K;
- the thermal contact between neighbouring slabs and the natural convection for aluminum slabs are absent, thus giving an upper limit of the core temperature.

3.2.1 Regular Operation Mode

In the regular operation mode the maximum density of an energy deposition in the aluminum core is equal to 0.28 J/cm^3 (Figure 2.5). It corresponds to the 0.12°C adiabatic temperature rise.

Steady state distributions of a temperature and an equivalent stress in the most heated slab are shown in Figures 3.2. The maximum temperature is equal to 59.2°C and is reached in approximately three and half hours. The maximum thermal stress arises inside the water cooling line and is equal to 13.2 MPa.

3.2.2 Emergency Mode

In the emergency (when the missteered primary beam does not interact with a target) the maximum density of an energy deposition in the absorber core is equal to 21 J/cm^3, what gives the 8.5°C adiabatic temperature rise.

The time of a thermal diffusion is defined as $t_d = \sigma^2/4a$ [4], where σ is the r.m.s. width of distribution of an energy deposition density and a is the thermal diffusivity ($a = \lambda/C_p d$, here λ is the heat conductivity, C_p is the specific heat and d is the density). Supposing that $\sigma \sim 7$ cm, one can get for an aluminum $t_d \sim 13$ s. Because this time is significantly larger than the repetition period of the Main Injector (1.9 s), the temperature and, correspondingly, thermal stresses will accumulate in the absorber core from spill to spill as it is shown in Figures 3.3 and 3.4. Distributions of a temperature and an equivalent stress in the most heated aluminum slab after 16 emergency spills, which occur at the steady state, are shown in

Figure 3.5. The temperature reaches the value of 129°C and the maximum equivalent stress in the aluminum slab increases up to 55.4 MPa. At the same time, 16 subsequent emergency spills do not increase the thermal load to a cooling system because the temperature gradient near the cooling line remains during this period unchanged (Figure 3.6).

The time constant τ of slab cooling may be estimated supposing that the temperature varies with time as $T \propto \exp(-t/\tau)$, where $\tau = t_0 T_{max}/\Delta T$, $t_0 = 1.9$ s is the Main Injector repetition period, T_{max} is the temperature after the last emergency spill and ΔT is the temperature change in t_0 after the last spill. Substitution of T_{max} and ΔT from Figure 3.3 gives $\tau \simeq 42$ s. It means that the absorber slab will be cooled in approximately 3–5 minutes.

3.3 Dynamical Stress in the Absorber Core in case of the Single Turn Extraction of a Primary Beam

The single turn extraction of a primary beam, which is now under serious consideration for NuMI, allows significantly decrease the losses of protons in the extraction area and downstream the proton beamline. The main difference of a single turn extraction from originally planed resonant extraction is the two order of magnidute shorter beam spill (8 μs instead of 0.5–1.0 ms). Concerning the absorber core design, all results given above for the resonant extracted beam will also take place in case of the single turn extraction, but in stress calculations it is necessary to take into account dynamical components.

An analytical consideration shows that the amplitude of a dynamical stresses is:

$$S_{xx}, S_{yy}, S_{zz} \sim \frac{2E\alpha T_0 \sigma}{(1-\nu)V_s t_p},$$

where E is the modulus of elasticity, α is the coefficient of thermal expansion, ν is the Poisson ratio, T_0 is the adiabatic temperature rise, σ is the r.m.s. width of the beam distribution, V_s is the sound velocity and t_p is the beam pulse duration. This expression reflects all main features of dynamical stresses, i.e.:

- for given core material and parameters of a beam, very short pulses may induce large dynamical stresses;
- the value of dynamical stresses is proportional to the total energy absorbed in a material ($T_0\sigma$).

Dynamical stresses were calculated by the ANSYS solving the three-dimensional task of elastic oscillations in the most heated aluminum slab of an absorber core. Transverse distributions of an energy deposition density in the absorber core were calculated assuming that the emittance of a single turn extracted beam in the horizontal direction is approximately two times larger than that for a resonant extracted beam. This is most pronounced in case of direct strike of the absorber by missteered proton beam: along with increasing of the r.m.s. width of its distribution in the horizontal direction, the energy deposition density at the beam axis in the most heated aluminum slab decreases from 21 J/cm^3 (Figure 2.8) up to 14 J/cm^3.

Results of dynamical stress calculations are given in Figure 3.7. In the regular operation mode the maximal equivalent dynamical stress is equal to 0.4 MPa and is essentially lower than the static thermal stress (9.5 MPa). Dynamical stresses in the emergency were calculated for the first emergency spill at the steady state of regular operation. Calculations show, that the dynamical stress reaches its maximum values at the beam axis and does not depend on the beam axis position on the face of an absorber core. Excluding the static stress of 13 MPa, the first peak of the equivalent dynamical stress is 11 MPa, while the following peaks are slightly less, what may be explained by coupling of axial and transverse oscillations via the Poisson ratio.

The analysis also shows, that spectra of all stresses contains the frequencies corresponding to following fundamental cyclic frequencies of slab elastic waves:

$$\Omega_k = \frac{\pi V_s k}{R}, \qquad \Omega_m = \frac{\pi V_s m}{L}, \qquad \Omega_n = \frac{\pi V_s n}{R+L},$$

where $k, m, n = 1, 2...$, $V_s = \sqrt{E(1-\nu)/d(1-2\nu)(1+\nu)}$, $2R$ is the width (height) of the absorber core and $2L$ is its length along the beam.

One should note, that the damping of oscillations was not taken into account in ANSYS calculations, but may be estimated in term of Q-value of oscillations. For given Q-value (usually $\sim$100–200), the time constant of damping is $\tau = 2Q/\omega$, where ω is the cyclic frequency of oscillations. The period of main frequency of S_{zz} oscillations is equal to 50 μs and hence $\tau \simeq$1.5–3 ms.

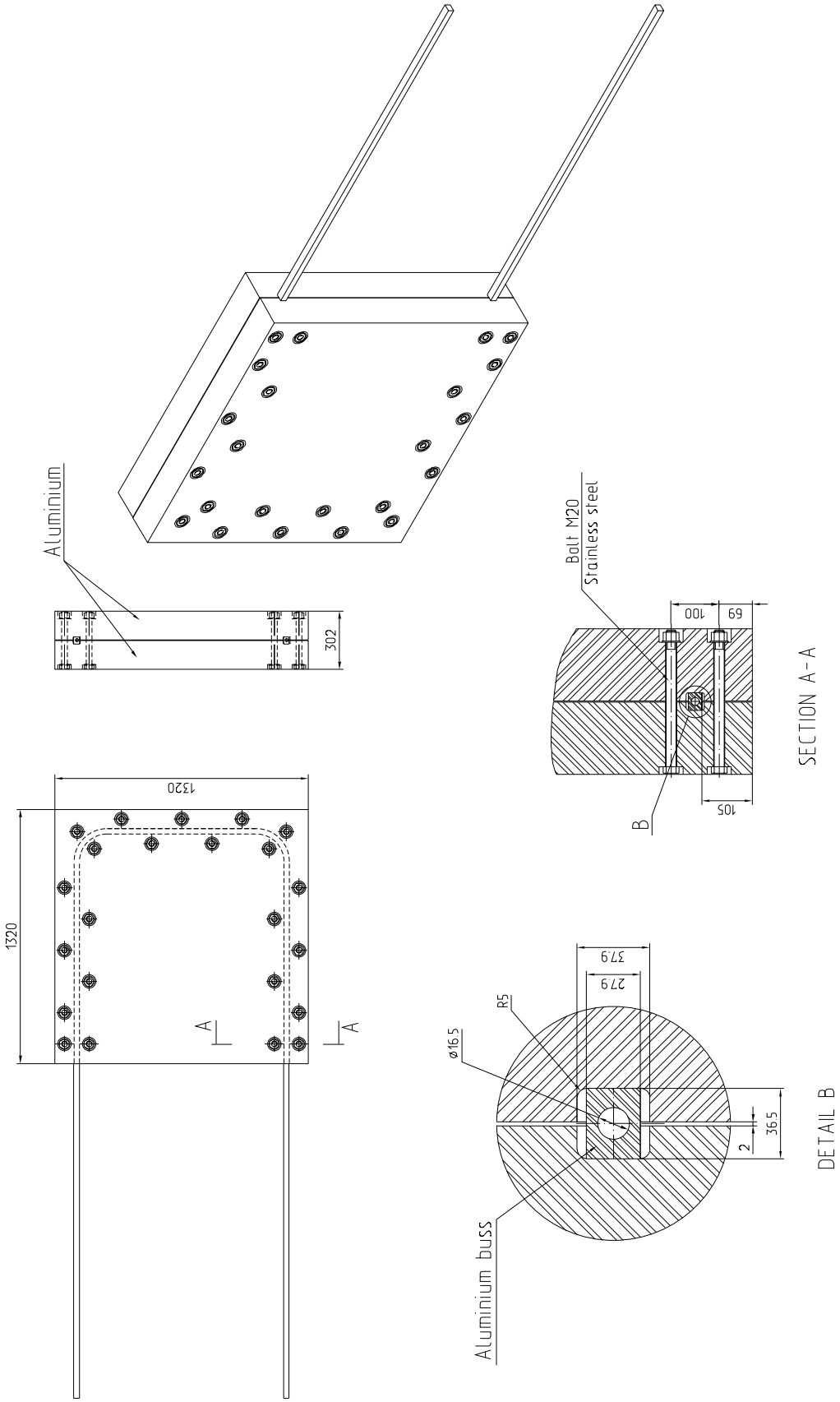

Figure 3.1: General view of the absorber core module design.

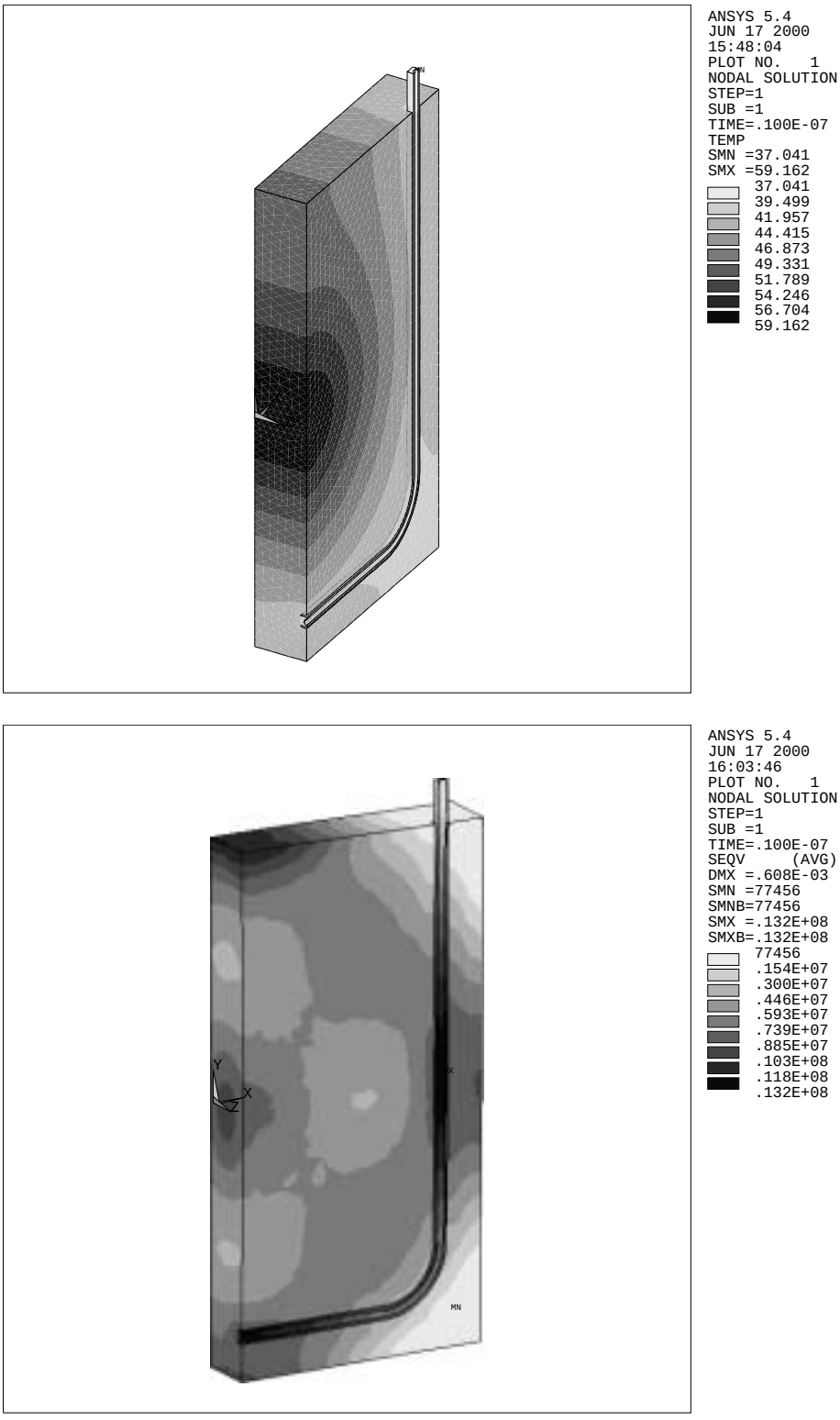

Figure 3.2: Steady state temperature (top) and stress (bottom) distributions in the most heated aluminum slab in the regular operation mode.

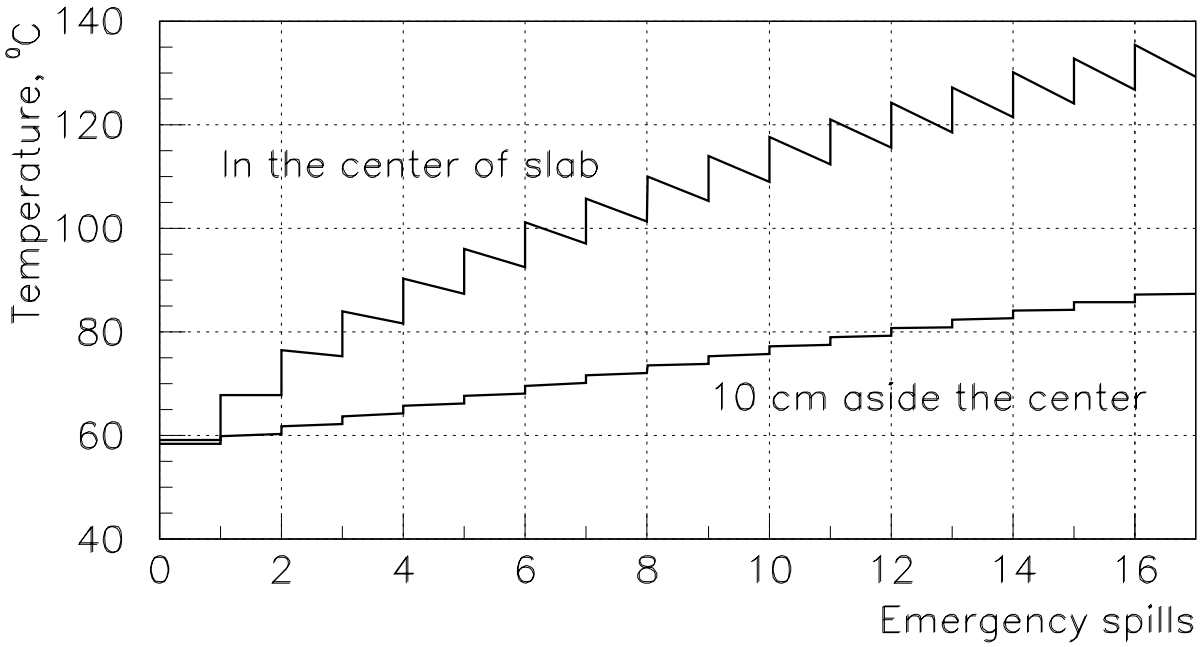

Figure 3.3: Spill to spill evolution of temperatures in two points of the most heated aluminum slab in the emergency.

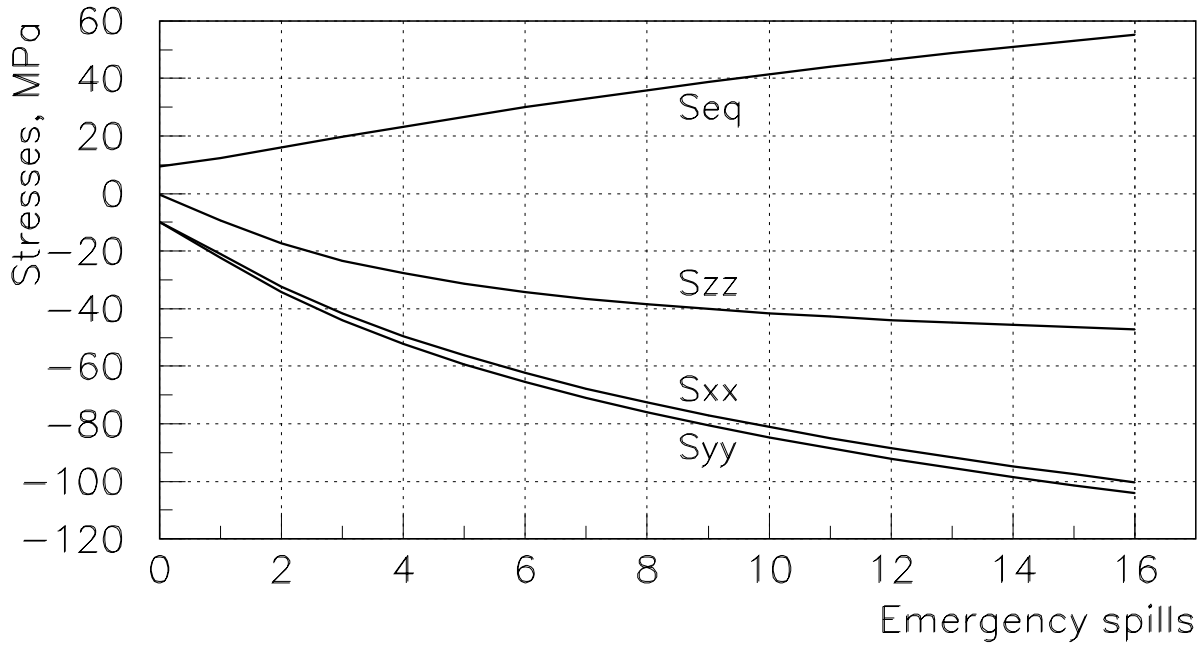

Figure 3.4: Spill to spill evolution of stresses in the center of the most heated aluminum slab in the emergency.

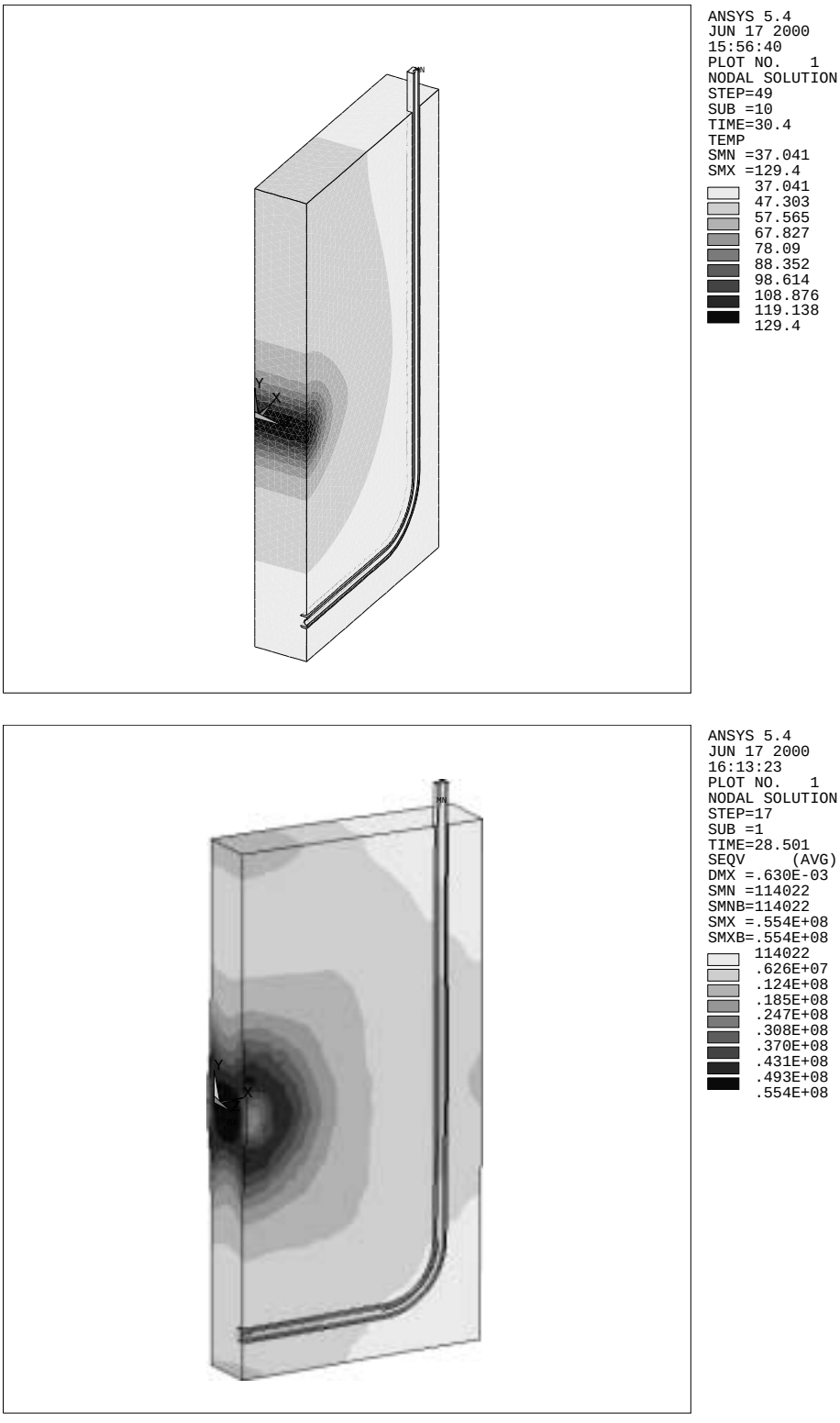

Figure 3.5: Temperature (top) and stress (bottom) distributions in the most heated aluminum slab after 16 subsequent emergency spills.

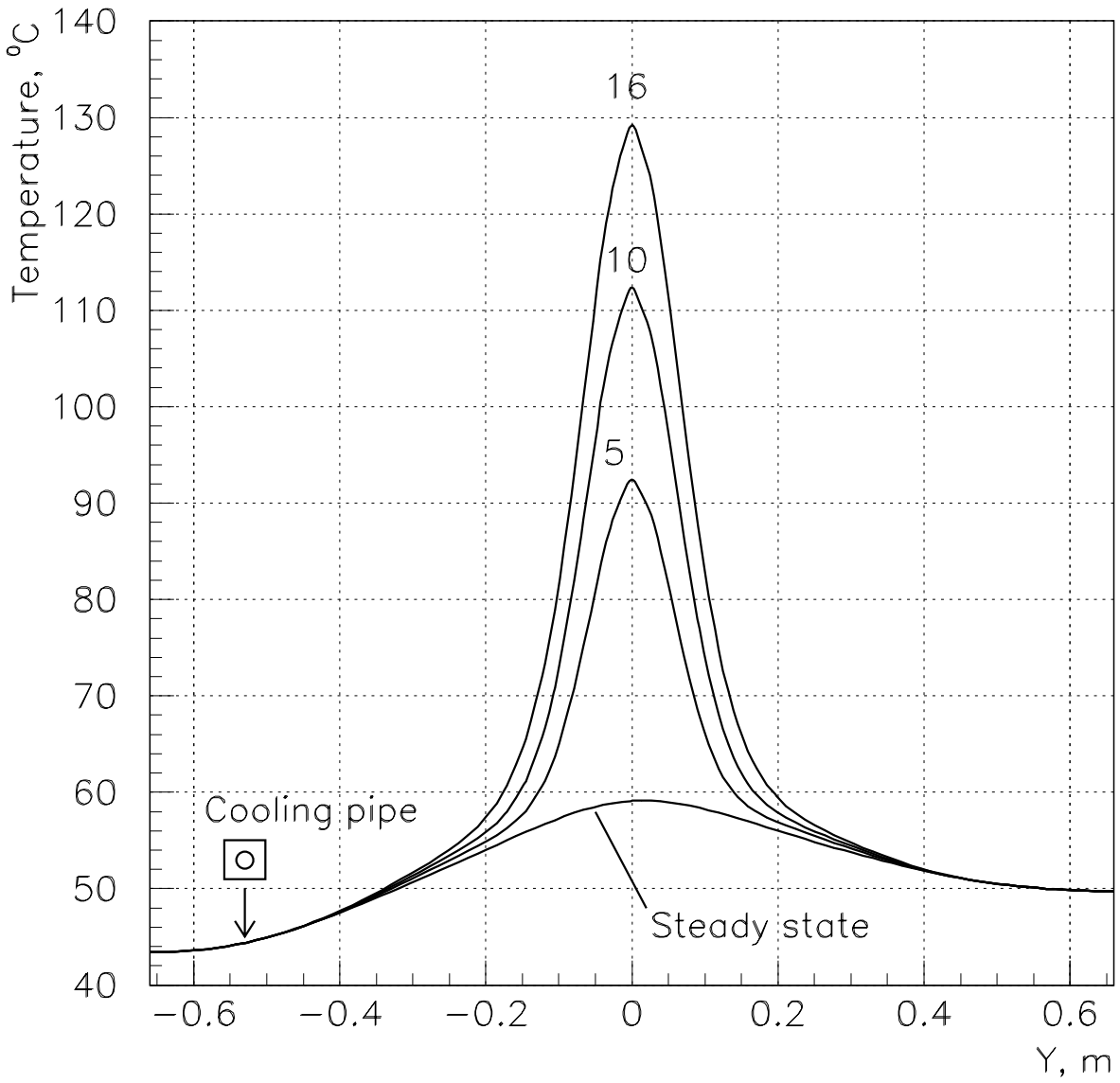

Figure 3.6: Temperature distributions along the vertical axis at the external surface of the most heated aluminum slab after 5, 10 and 16 subsequent emergency spills.

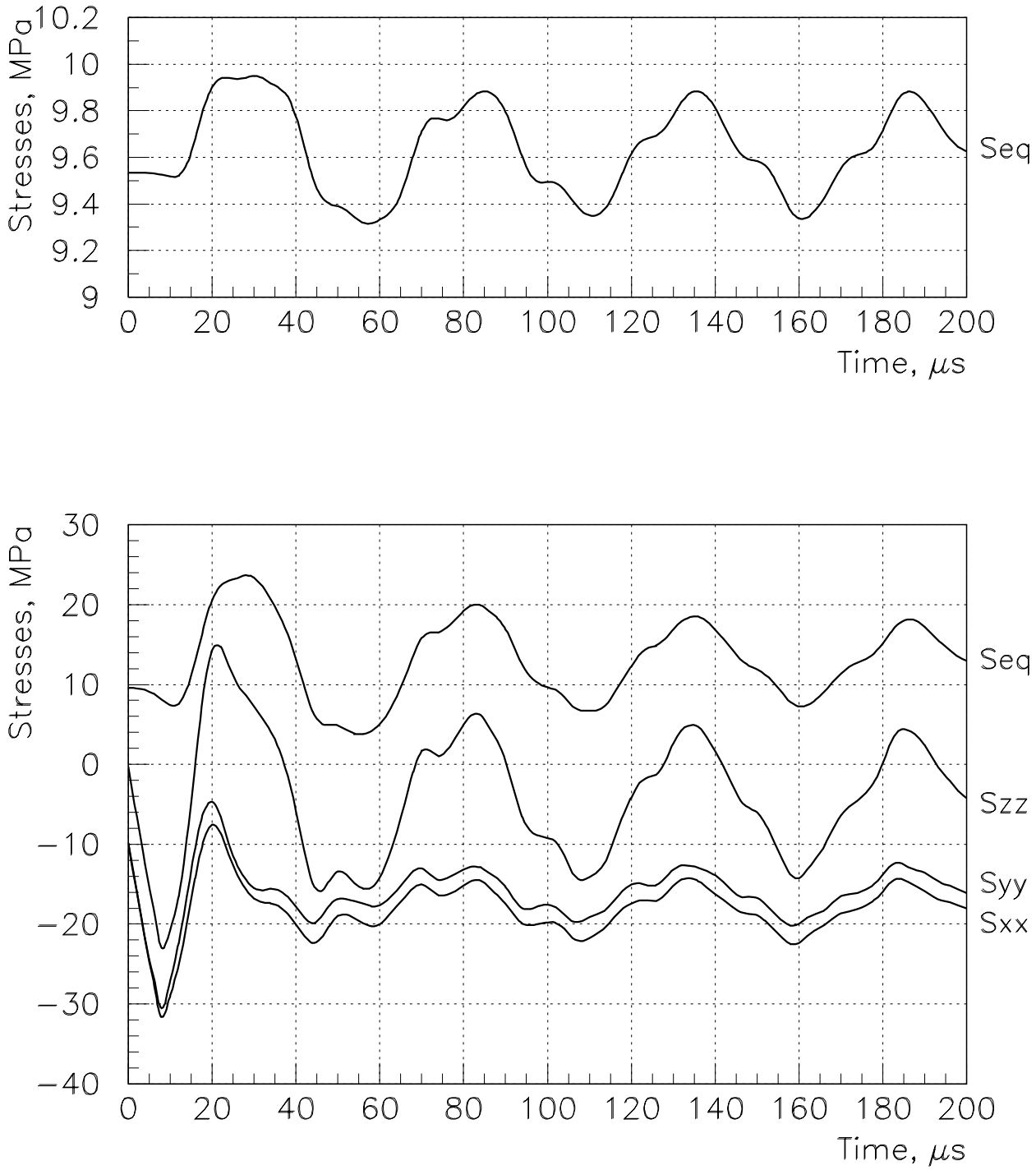

Figure 3.7: Time evolution of stresses in the center of the most heated aluminum slab in the regular operation mode (top) and in the emergency (bottom) in case of the single turn extraction of a primary beam.

4 Some Engineering Problems of the Core Design

4.1 Aluminum Grades for the Absorber Core

The choice of an aluminum grade for the core design should take into account temperatures and thermal stresses, which arise in an absorber core during its operation (Table 4.1).

Beam spill duration	1 ms	8 μs
Static stress at the regular operation, MPa	9.5	9.5
Max. temperature at the regular operation, °C	59.2	59.2
Static stress after 16 emergency spills, MPa	55.2	54.9
Max. temperature after 16 emergency spills, °C	135	123.6
Dynamical stress at the regular operation, MPa	0	0.4
Dynamical stress at the emergency, MPa	0	11

Table 4.1: Results of ANSYS calculations of temperatures and thermal stresses in the absorber core.

Among the variety of aluminum alloys two grades with proper thickness of plates are available from industry [5]: 1100 and 5052. Grade 5052 is $\sim$2 times stronger than grade 1100. Grade 1100, which is considered below as a possible material for the absorber core, is available in following modifications: 1100-O, 1100-H12, 1100-H14, 1100-H16 and 1100-H18.

Extension "O" means annealed and applies to wrought products which are fully annealed to obtain the lowest strength temperature and to cast products which are annealed to improve ductility and dimensional stability.

Extension "H" means strain–hardened (wrought products) and applies to products which have their strength increased by strain–hardening with or without supplementary thermal treatments to produce some reduction in strength. The "H" is always followed by two or more digits and larger number corresponds to greater strength.

The most full data are available for grades 1100-O and 1100-H14, i.e. besides of typical properties in [5] are given their dependencies on the temperature and for grade 1100-H14 in addition the data on minimal mechanical properties are given too. Thermal and mechanical properties of these grades are presented in Table 4.2 and in Figure 4.1.

Aluminum alloy	1100-O	1100-H14
Modulus of elasticity, GPa	69	69
Ultimate tensile strength, MPa	83	124 (110)
Yield stress, MPa	28	117(97)
Fatigue endurance limit ($5{\cdot}10^8$ cycles), MPa	21	48
Heat conductivity, W/m·K	222	222
Average coefficient of thermal expansion (20–100)°C, 10^{-6}1/K	23.6	23.6

Table 4.2: Mechanical and thermal properties of aluminum alloys. Values in brackets are minimal guaranteed.

The regular operation mode. At the steady state of a regular operation the stresses for both types of the beam extraction are equal to 9.5 MPa, what is essentially lower than yield stresses of considered aluminum grades. The sum of static and dynamical stresses in case of the single turn extraction is also essentially lower than the fatigue endurance limit. Therefore the grade of an aluminum alloy for the absorber core should be chosen based on results of stress calculations in the emergency.

The emergency. In the emergency the maximal temperature in the absorber core increase, therefore it is necessary to take into account variation of mechanical properties of an aluminum with a temperature. Supposing that the emergency occurs rarely, the low cycle fatigue limit is naturally to use for the estimation of a core material workability. There are no data on the low cycle fatigue tests in [5]. Compilation of data for Russian aluminum alloys [6] shows that for the test base of 50000 cycles the low cycle fatigue limit S_{max} is approximately equal to 50% of the ultimate strength (S_{max} increases with decreasing of the number of test cycles).

Figure 4.2 gives S_{max} in an approach of 0.5 from the ultimate strength at various temperatures and the equivalent thermal stress as a function of the core temperature for the resonant extraction of a primary beam (combination of data shown in Figures 3.3 and 3.4). The same dependence is given also for the single turn extraction taking into account the dynamical stress. As it follows from these plots, the choice of considering aluminum grades depends on the number of allowable emergency spills. One should note, that this estimation is valid for the 50000 emergency situations, i.e.

for example, the series from 5 emergency spills of a single turn extracted beam for the aluminum grade 1100-O may be repeated 50000 times.

4.2 Dimensions of Cooling Pipes

Three types of aluminum busses available from the industry were considered as possible cooling pipes for the absorber core module. Their dimensions and calculated parameters of cooling for the most heated module (~8 kW) are given in Table 4.3.

Buss dimensions, H×V mm^2,ϕ mm	38.1×27.9, 16.5	35.6×35.6, 15.9	31.0×18.3, 10.2	
Water velocity, m/s	2	2	2	5
Water flow rate, l/min	25.7	23.8	9.8	24.5
Film coefficient, $kW/m^2 \cdot K$	8.5	8.6	9.2	20.0
Water temperature rise, °C	4.5	4.8	11.7	4.7
Pressure drop, atm.	0.27	0.28	0.48	2.7
Water-"wall" temperature rise, °C	3.0	3.1	4.5	2.1

Table 4.3: Dimensions of aluminum busses and parameters of cooling.

One should note, that at the water velocity equal to 5 m/s, the water temperature rise in the third buss is approximately the same as for first two busses at the water velocity of 2 m/s, but the product of a pressure drop and a water flow rate (the value proportional to the power of a water pump) is ~10 times larger. The last line in Table 4.3 gives the temperature rise between a water and cooling pipe walls, which exist due to the finite value of a film coefficient and the limited area of heat exchanging between slabs and a cooling pipe.

The analysis of data given in this Table shows, that first two busses are preferable for using as a cooling pipe for the core module. Taking into account that the MINOS Near Detector coil is being made of an aluminum buss with dimensions of 38.1×27.9 mm^2, it is reasonable to use this buss as a cooling pipe for the core module too.

4.3 Contact Thermal Conductance between the Cooling Pipe and Slabs

According to Yovanovich and Slykov models [7, 8], the total contact thermal conductance is the sum of two parallel and independent conductances: the

medium (gas) conductance a_g and the solid–solid contact conductance a_s, i.e. $a_{tot} = a_g + a_s$. For given average roughness h_1, h_2 of two contacting surfaces a_g and a_s may be defined by semi–empirical expressions [8, 9]:

$$a_g = \frac{Y\lambda_g}{2(h_1 + h_2 + \delta)} \quad ,$$

where λ_g is the gas heat conductivity, Y is the coefficient, which depends on the way of machining of contacting surfaces and lies in the range of 2.0–3.3, $\delta/2$ is the average air gap between two contacting surfaces (this gap may be caused, for example, by the nonflatness of contacting surfaces);

$$a_s = 8 \cdot 10^3 \lambda_s \Big(\frac{P}{3S_{ft}} K\Big)^{0.86},$$

where $\lambda_s = 2\lambda_1\lambda_2/(\lambda_1 + \lambda_2)$, λ_1 and λ_2 are heat conductivities of contacting metals, P is the contacting pressure, S_{ft} is the minimum ultimate strength of contacting metals, K is the nondimensional constant which depends on roughness (μm):

$$\begin{array}{llll} K = 1 & \text{if} & 30\mu m \leq & (h_1 + h_2), \\ K = (30/(h_1 + h_2))^{0.33} & \text{if} & 10\mu m \leq & (h_1 + h_2) \quad \leq 30\mu m, \\ K = (15/(h_1 + h_2)) & \text{if} & & (h_1 + h_2) \quad \leq 10\mu m. \end{array}$$

Note that these expressions may be used only for "metal–to–metal" contacts and are limited to values of $P/3S_{ft}$ of about 0.02–0.025 and temperatures lower than $0.3T_{melt}$. Note also that numerical constants in expressions for a_g and a_s are in m^{-1}.

A good thermal contact between slabs and cooling pipe will be reached in case of the solid "metal–to–metal" contact, i.e. when contacting surfaces are ideal planes with given roughness. In this case at the contact pressure of 3 MPa and the 15 μm roughness of contacting surfaces, the thermal conductance of the "slab–to–cooling pipe" contact may be estimated as 4.2×10^4 W/m^2·K [8, 9]. It corresponds to the $\sim$1°C temperature rise between the most heated slab (3.9 kW) and the cooling pipe.

At the assembly pressure of 3 MPa, cooling pipes, as well as the slab deform elastically and average nonplanarity of contacting surfaces more than 4 μm can not be compensated during an assembly. Because of very "long" contact, some its region will have a pure gas conductance. Using the expression for a_g, one can get $a_g = 330$ W/m^2·K for the 50 μm average

nonflatness. This value is ∼125 times lower than the solid thermal conductance a_s, what lead to high requirements to the nonplanarity of slabs and cooling pipes (in order of or better than the roughness). There are two ways to decrease an accuracy of slabs and cooling pipes machining, and, at the same time, to achieve a good contact thermal conductance.

1. The assembly of a cooling pipe and slabs should be preliminary exposed to a plastic deformation in the ∼300 tons press. If the yield strength of a pipe material is lower than the yield strength of a slab material, mainly the cooling pipe will deform plastically. After a plastic deformation, the cooling pipe can be clamped between two slabs with help of steel bolts. The exact knowledge of elastic and plastic properties of a pipe material is necessary in this case for an estimation of the accuracy of cooling pipe and slabs machining, as well as the value of a pressing force.

2. According to [8], an increase of a solid thermal conductance can be achieved with help of an intermediate layer from a metal with the plasticity higher than the plasticity of contacting metals. The indium (In), which in the Periodic Table of elements is located in the same valence group as an aluminum, may be used as such layer between a cooling pipe and slabs. In this case the accuracy of cooling pipe and slabs machining may be essentially lower with respect to the design without an intermediate layer and may be specified as 0.1–0.2 mm. The similar accuracy may be specified and for the nonflatness of drain in the slab. Taking into account the ultimate compressive strength of indium, the pressure between the cooling pipe and aluminum slabs may be specified as ∼3 MPa.

4.4 Material of Bolts

Cooling of steel bolts, which are used for clamping of a cooling pipe between two aluminum slabs, will be effected by two processes:

- the heat exchange through the air gap between bolts and aluminum slabs. The heat transfer coefficient for this process may be calculated using given above formula for a_g;
- the heat exchange between bolts and aluminum slabs due to the heat conductivity of steel.

Taking into account both processes of cooling and solving the differential equation of a heat conductivity $div(\lambda gradT) + Q_v = 0$, where λ is the heat conductivity of steel and Q_v is the volume heat source obtained from MARS energy deposition calculations; one can get:

$$T(x) = Q_v \frac{R}{2a_g}\left(1 - \frac{\cosh(\omega x)}{\cosh(\omega L)}\right) + T_{al},$$

where $\omega = \sqrt{2a_g/\lambda R}$, x is the distance from the bolt center, L is the bolt half length and R is the bolt radius, T_{al} is the temperature of surrounding aluminum. Elongations of a steel bolt and aluminum slabs are defined as:

$$\frac{\Delta L_s}{L} = \alpha_s(\widetilde{T} - T_0) + \delta_s, \qquad \frac{\Delta L_{al}}{L} = \alpha_{al}(T_{al} - T_0) + \delta_{al},$$

where $\widetilde{T} = \frac{1}{L}\int_0^L T(x)dx$ is the average temperature of a bolt, T_0 is the temperature during the core module assembly, α_s and α_{al} are coefficients of thermal expansion of a steel and an aluminum respectively, elongations δ_s and δ_{al} are caused by the additional thermal force F_b, which arises in the bolt and in Hook approach may be calculated as:

$$F_b = \left(\frac{1}{E_s \pi R^2} + \frac{1}{E_{al} S_{al}}\right)^{-1} \left(\alpha_s(\widetilde{T} - T_0) - \alpha_{al}(T_{al} - T_0)\right),$$

where E_s and E_{al} are moduluses of elasticity of a steel and an aluminum respectively, S_{al} is the average per one bolt contact area of a cooling pipe and an aluminum slab.

To examine the influence of steel properties on the parameters of bolted connection of two aluminum slabs, three Russian steel grades with different coefficients of thermal expansion and heat conductivities were considered as possible bolt materials. The CT20 grade is a high quality carbon steel, 30ХГС is a structural grade of moderate strength and 12Х18Н10Т is a widely used stainless steel. Their properties are given in Table 4.4.

Steel grade	СТ20	30ХГС	12Х18Н10Т
Heat conductivity, W/m·K	86	39	15
Coeff. of thermal expansion, 10^{-6} 1/K	11.1	11.3	17.5
Yield strength, MPa	250	900	220
Ultimate tensile strength, MPa	430	1100	550

Table 4.4: Properties of Russian steel grades.

Distributions of temperature along the bolt for these steel grades, calculated with help of given above expression[6] for $R = 10$ mm, $L = 150$ mm and $Q_v = 0.0145$ W/cm^3, are given in Figure 4.3. The thermal forces arising in bolts as functions of the difference in temperatures during the assembly and operation are given in Figure 4.4 in comparison with the nominal force of 13.5 kN providing the 3 MPa pressure on the cooling pipe. In spite of the difference in thermal conductivities, steel grades CT20 and 30ХГС give practically the same thermal forces, what may be explained by the fact that thermal force is defined mainly by the difference in coefficients of thermal expansion of a steel and an aluminum.

The problem, which significantly affect a bolt material choice, is the large difference between the temperature during the module assembly T_0 and the operational temperature of an aluminum T_{al}. At the cooling water temperature of 37°C, the operational temperature of an aluminum at the location of bolts is about 43°C, thus $T_{al} - T_0 \simeq 23$°C at the $T_0 = 20$°C.

Any considered steel grade may be chosen as a bolt material, if the core module assembly does not use indium layers between a cooling pipe and slabs. In this case the force applied to a bolt should be determined taking into account mechanical properties of slab, cooling pipe and bolt materials, as well as additional thermal forces which arise in bolts (Figure 4.4).

For the core module assembly with intermediate indium layers, the bolt material and the applied force should be determined taking also into account the ultimate compressive strength of indium (~3 MPa). Under mentioned above temperatures the stainless steel 12X18H10T gives the thermal force equal to 5.3 kN, whereas two other steel grades give significantly larger forces which are undesirable for clamping of aluminum slabs with indium layers. The force applied to the 12X18H10T stainless steel bolt during the module assembly should be equal to 8.2 kN, while the rest to the nominal force will be provided by the thermal force arising in a bolt. Calculations of stresses in the bolt and the nut show, that at the nominal force the values of crushing stress (24 MPa), cutting stress (17.2 MPa) and tensile stress (57 MPa) are significantly smaller than strength parameters of a material (Table 4.4), thus the stainless steel may be used as bolts and nuts material for clamping of aluminum slabs.

[6] ANSYS calculations for the 30ХГС grade give the ~0.01°C difference in the bolt temperature.

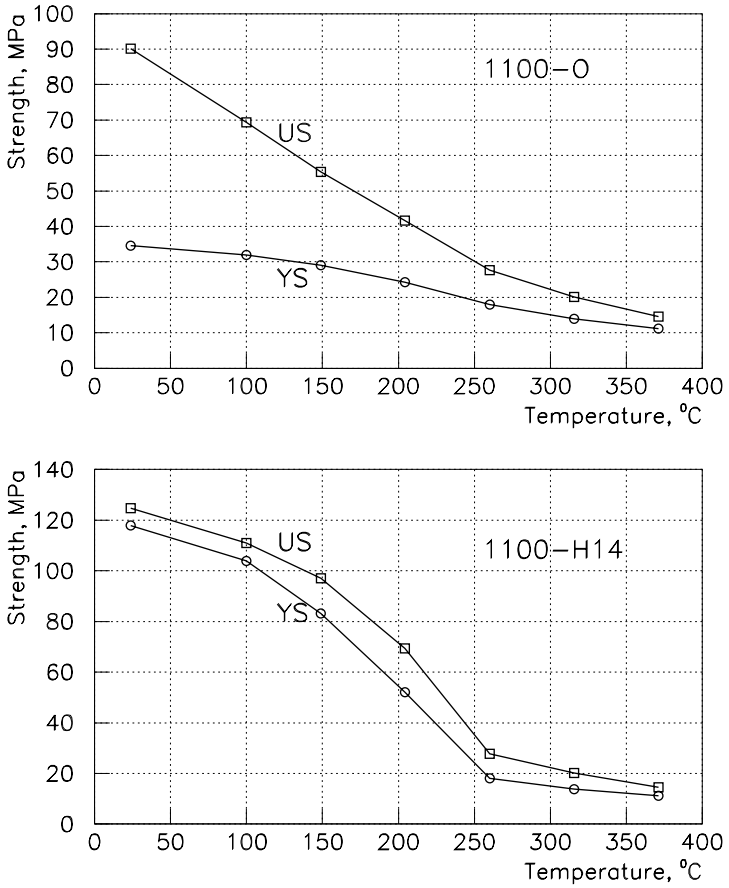

Figure 4.1: Typical tensile properties of aluminum grades at various temperatures. US — ultimate strength, YS — yield strength.

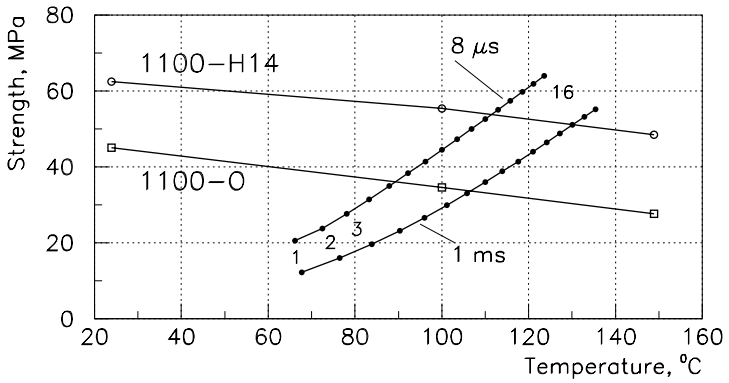

Figure 4.2: Low-cycle fatigue limits of aluminum grades at various temperatures and dependencies of equivalent stresses on a temperature in the center of the most heated aluminum slab in the emergency for two types of extraction. Numbers alongside these lines mark emergency spills.

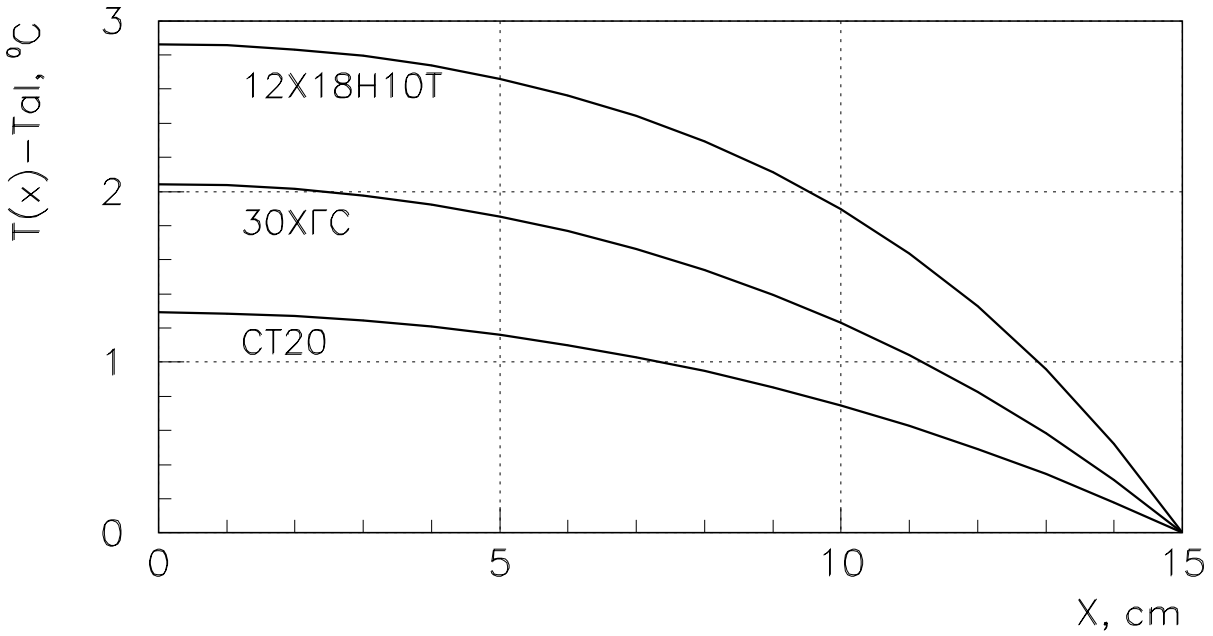

Figure 4.3: Temperature distributions along the bolt length for three different steel grades.

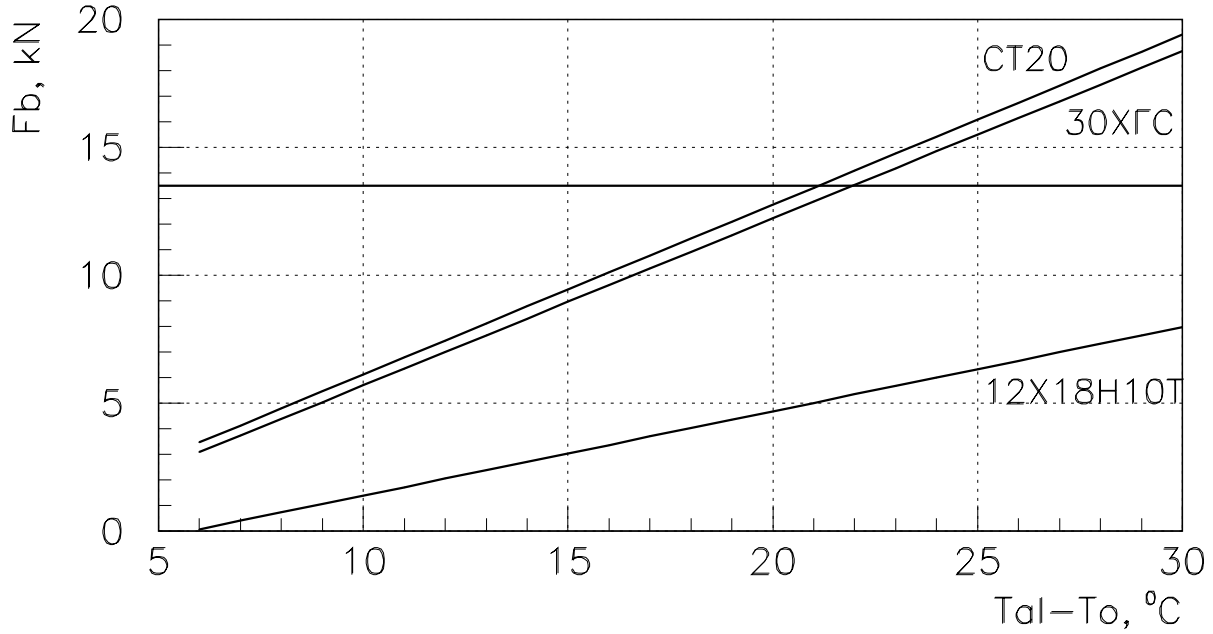

Figure 4.4: Thermal forces in bolts as functions of the difference in temperatures during the assembly and operation for three steel grades in comparison with the 13.5 kN nominal force.

5 Cooling of Steel Shielding

Results of MARS energy deposition calculations in steel shielding of the absorber, discussed in section 2.2.2 and given in Figures 2.3, 2.4 and 2.6, were used for ANSYS calculations of a steel temperature. Because of the block structure of shielding, the main problem in calculations of a steel temperature is the definition of boundary conditions. Therefore temperature calculations of steel shielding were made at the boundary conditions chosen in such a way to obtain an upper limit of a temperature.

5.1 Temperature of Steel Shielding behind the Absorber Core

Accordingly to MARS results, the 4.1 kW of a beam power is deposited in the first 0.3 m steel slab located behind the aluminum core. Because this block is located inside the absorber, it is not so easy to define the air convection coefficients and thus to predict its temperature correctly in case of air convection cooling. To be sure that the temperature of this steel slab will not be very large, it is reasonable to use for its cooling a water system. The design of the water cooled steel block may be exactly the same as for the aluminum core module. Figure 5.1 gives the temperature distribution in the water cooled steel block calculated at the boundary conditions used previously for temperature calculations in the aluminum slab (without the natural convection and the thermal contact between neighbouring slabs). The maximum temperature at the steel surface is equal to 89°C.

The temperature distribution in the steel block with nominal dimensions ($1.32 \times 1.32 \times 0.66$ m^3) located behind the water cooled steel block were calculated under the following boundary conditions:

- there are 1 mm air gaps between all steel slabs and between the lower slab and the floor. The heat exchange between two neighbouring slabs is only due to the air heat conductivity;
- air convective cooling exists only on the external surface of steel shielding. Convection coefficients were calculated by semi-empirical formula and were taken 25 W/m^2·K at lateral sides and 10 W/m^2·K at the upper side of shielding;
- floor and ambient temperatures are equal to 20°C.

Results of temperature calculations for this steel block are given in Figure 5.2. Under these boundary conditions the maximum temperature is equal to 91°C. This result may be used for an estimation of the temperature of the steel block with nominal dimensions in case when this steel block is located behind the absorber core and is not water cooled. Using the data from energy deposition calculations (Figure 2.4), one may expect ~3 times higher temperature.

5.2 Temperature of Steel Shielding around the Absorber Core

As it was mentioned in section 2.2.2, the main part of power deposited in steel shielding around the absorber core is deposited in first four blocks of nominal dimensions marked as 2, 4, 6 and 8 in Figure 2.3. The transverse distribution of deposited power which was used in ANSYS calculation is given in Figure 2.6. It was supposed that the steel block is cooled through the face surface with the convection coefficient of 20 $W/m^2 \cdot K$. The temperature distribution in the block 2 is given in Figure 5.3. The maximum temperature at the face of the steel block is equal to ~83°C.

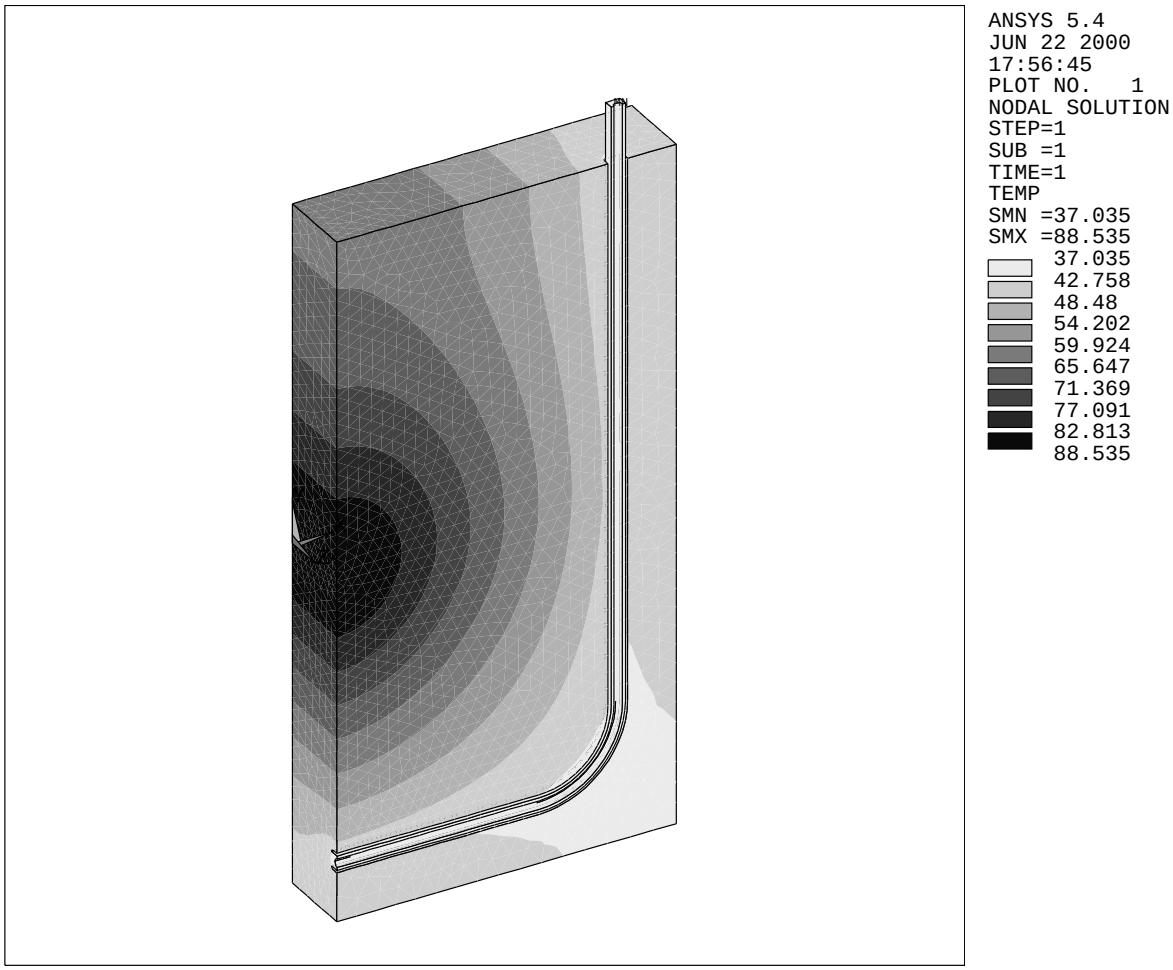

Figure 5.1: The temperature distribution in the water cooled steel block.

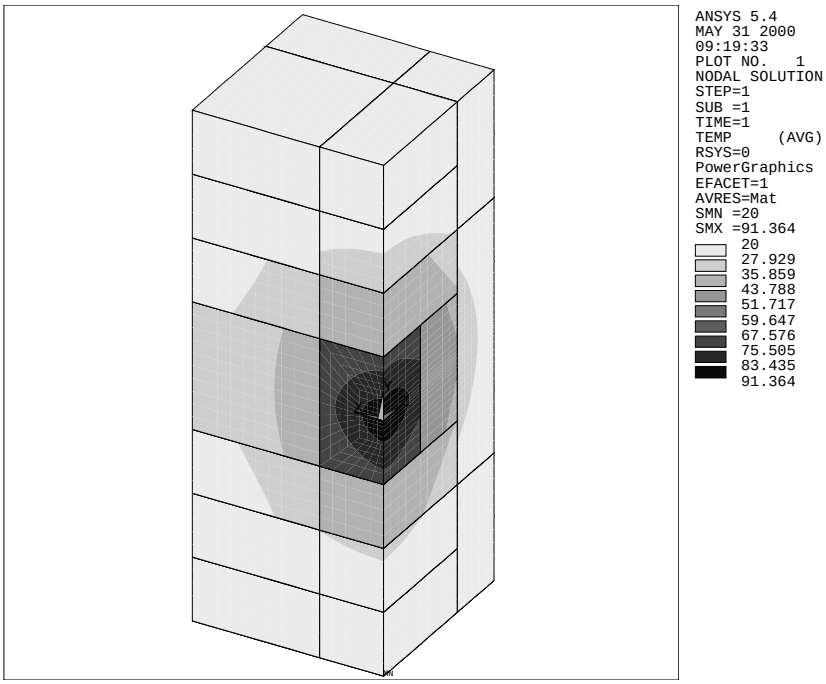

Figure 5.2: The temperature distribution in steel shielding located behind the water cooled steel block.

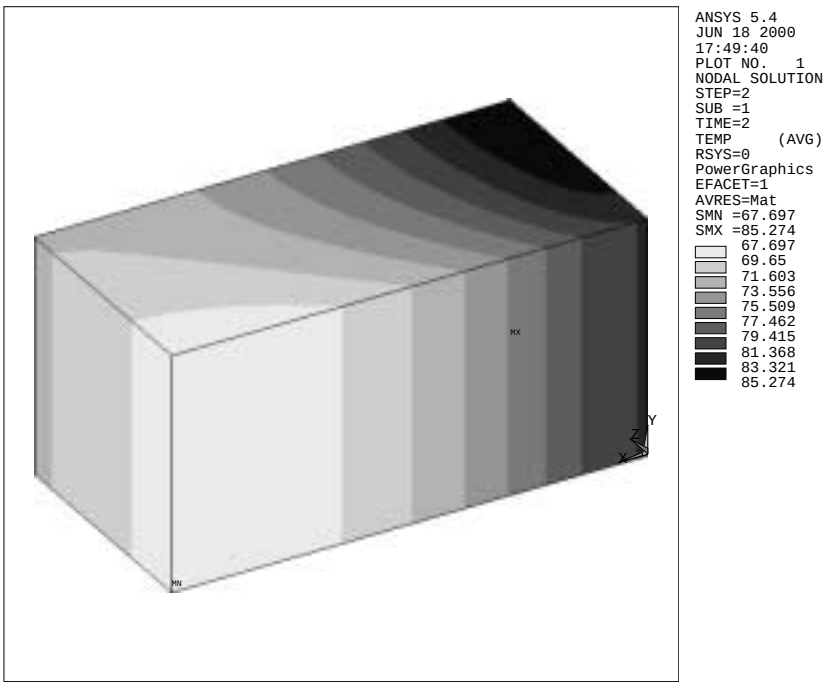

Figure 5.3: The temperature distribution on the steel block located at the upstream end of the absorber.

6 Design of the Absorber using "Filler Modules" Conception

The repair or change of the absorber core module are connected with the possibility of core dismantling in an Absorber Cavern without overhead crane. One and, it seems, unique possibility is removing of a failure module to the left (or right) with respect to the beam direction as it is shown in Figure 6.1. This is the attempt of realization of a "filler module with roller conveyor" conception.

Nine "filler modules" of an absorber (eight modules of an aluminum core and one water cooled module of steel shielding) may be removed for the repair or change. The dimensions of a removing module are chosen in such a way that the weight of each module does not exceed 10 tons. This conception may be used also for an installation of muon detectors. Main geometrical dimensions of the absorber are given in Figure 6.2 which shows the elevation cross-section of an absorber. Some details of the absorber assembly are given in Figure 6.3.

One should note, that long-term high intensity irradiation of the absorber core causes a large induced radioactivity of material, that will complicate any necessary operations with a failure core modules.

As it follows from energy deposition calculations, the average flux of high energy particles varies in the vicinity of the beam axis from 3.2×10^{9} $cm^{-2}\,s^{-1}$ in the first module up to 1.8×10^{10} $cm^{-2}\,s^{-1}$ in the fourth (most heated) core module, while at lateral sides of core modules the flux of particles is approximately 20 times lower.

Based on these results and data from [10, 11], preliminary estimations of expected dose rates from the surface of aluminum core modules were made under the assumption that the irradiation time is large than 50 days. Calculations show, that even at lateral sides of aluminum core modules the dose rate at the 10 cm distance from the surface reaches 5–20 R/hour after the 1 day cooling time and then decreases up to 0.2–1.0 R/hour after a month of cooling. Dose rates in the vicinity of beam axis are approximately 20 times higher.

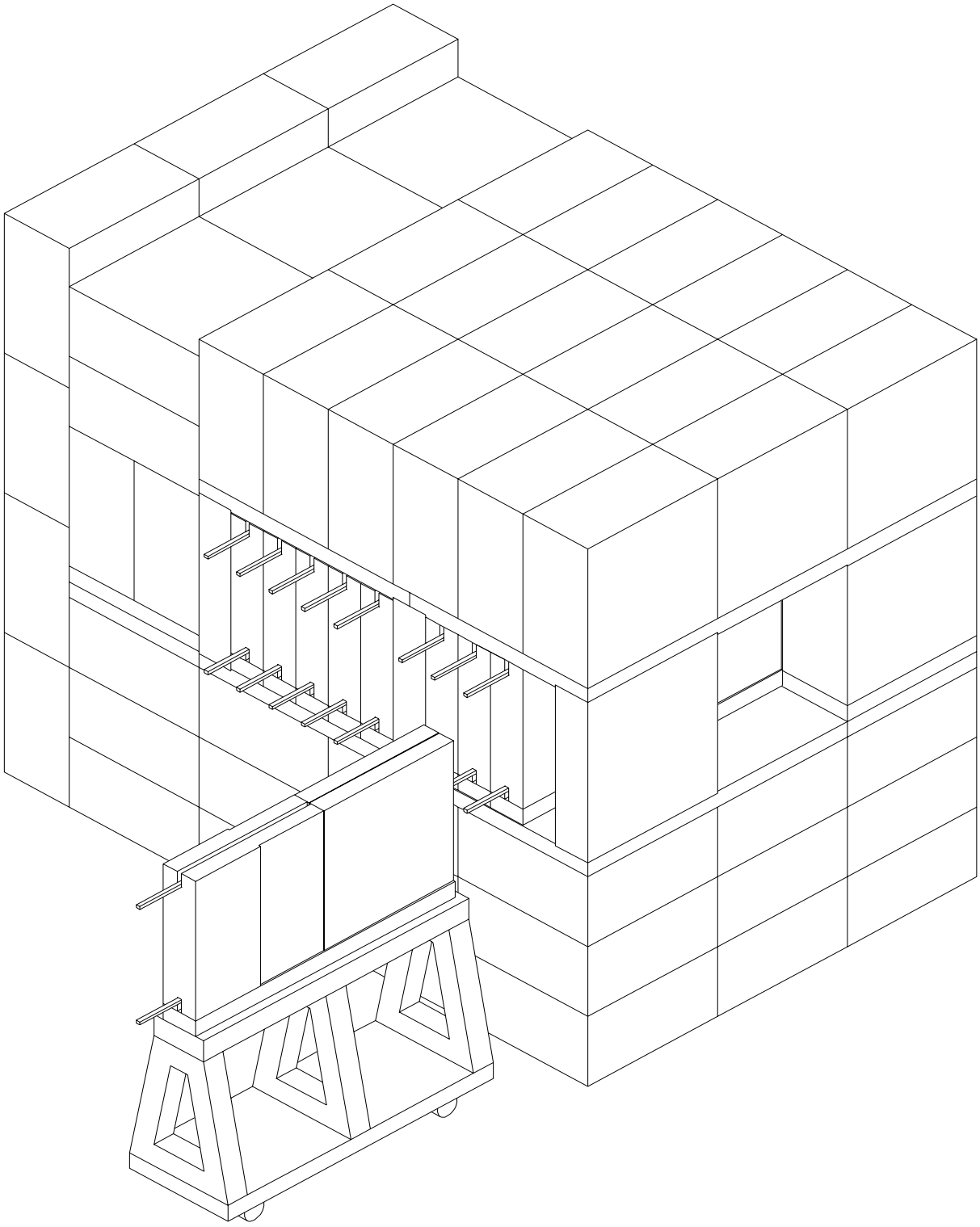

Figure 6.1: The general view of the absorber design using the "filler module with roller conveyor" conception.

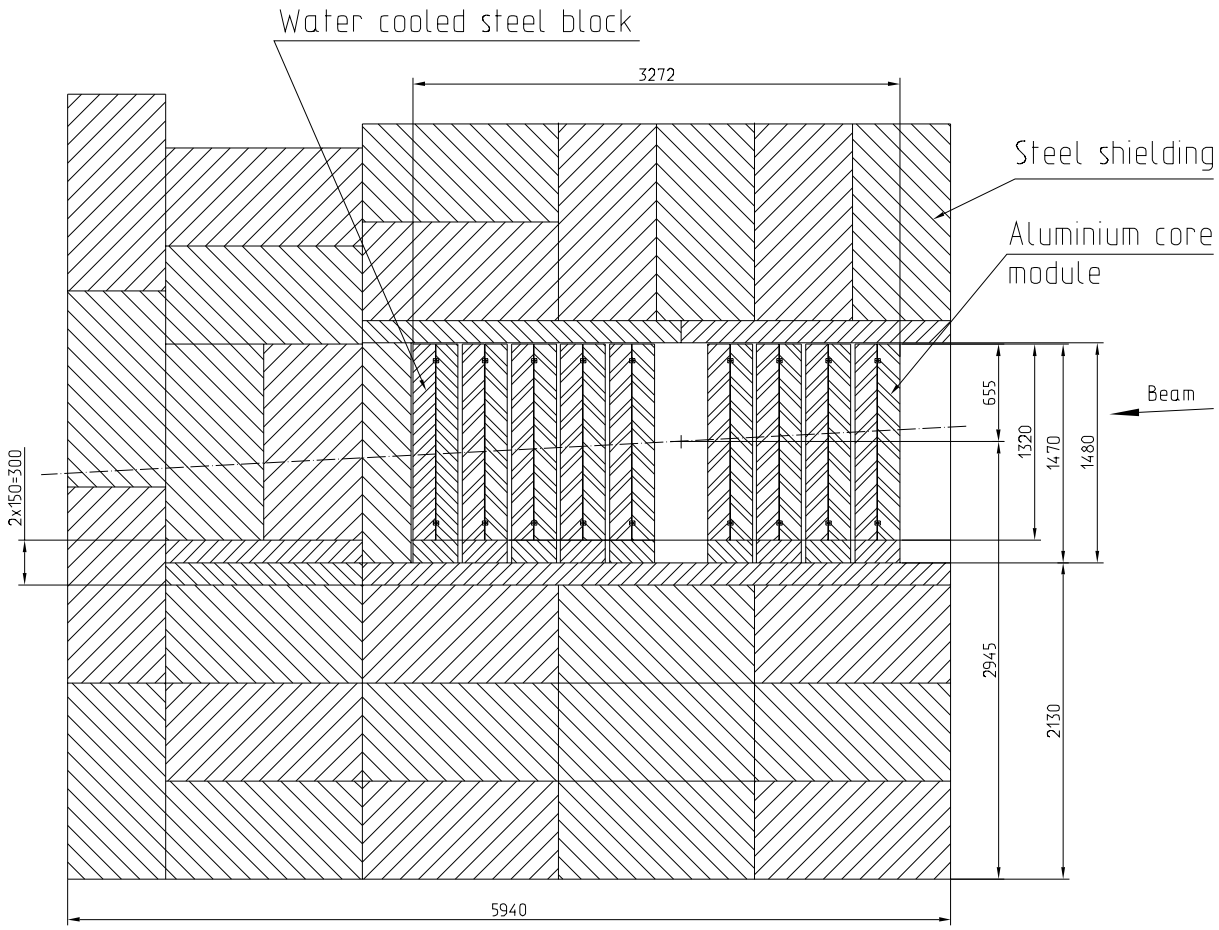

Figure 6.2: The elevation cross-section of the absorber.

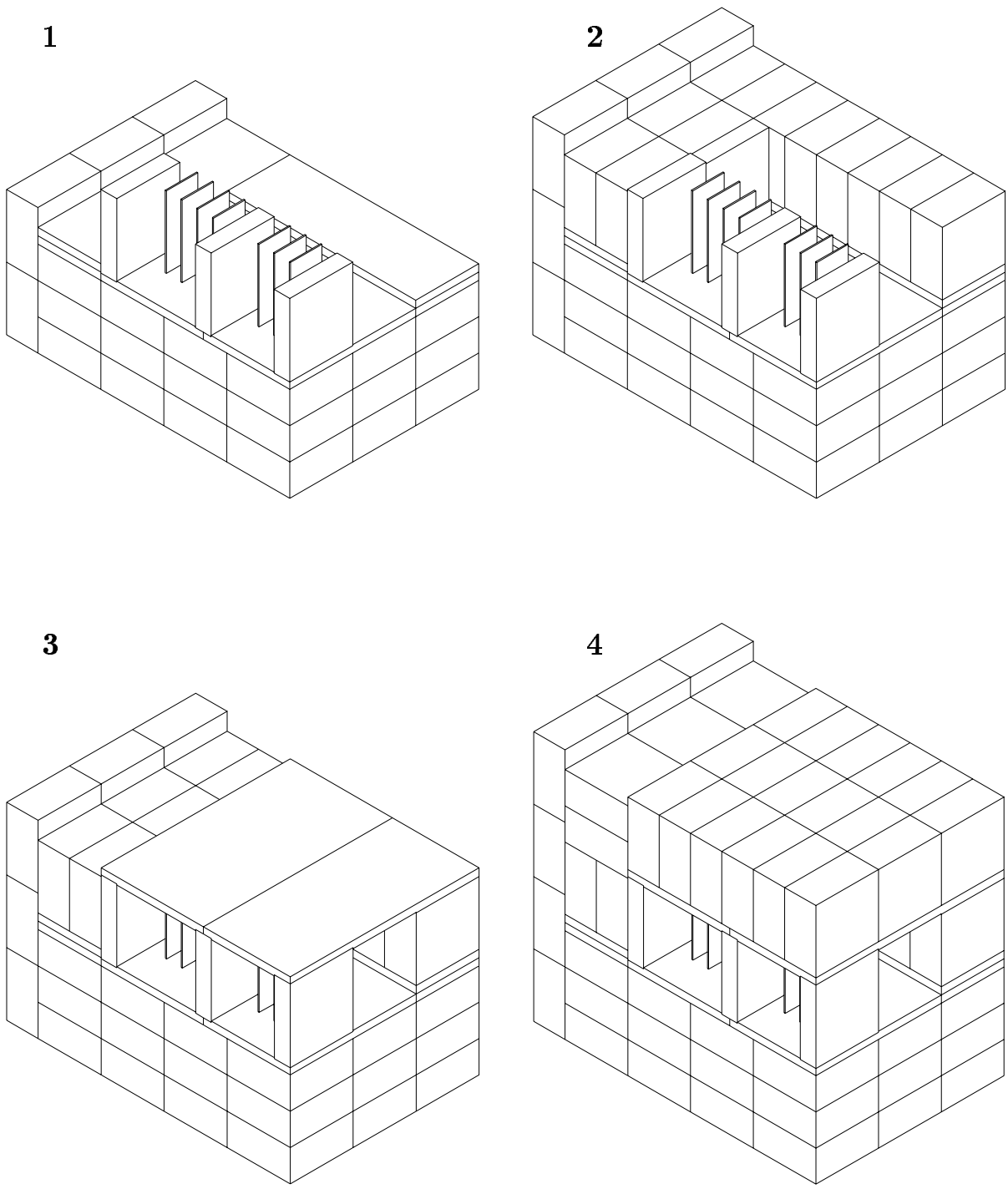

Figure 6.3: Main steps in the assembly of absorber shielding.

References

[1] The NuMI Facility Technical Design Report, Fermilab, 1998.

[2] I.Azhgirey et al., Procedings of XV Workshop on Charged Particles Accelerators, v.2, p.270, Protvino, 1996.

[3] J.Hylen et al., Proposal to Include Hadronic Hose in the NuMI Beam Line, NuMI-B-542, Fermilab, 1999.

[4] W.Kalbreier, W.Middelkoop, P.Sievers, CERN LAB II/BT/74-1, Geneva, 1974.

[5] Aluminum Alloys and Product Forms, A.Wehmann's FAX from April 4, 2000.

[6] I.Grigorieva, E.Meilikhova, Physics values, Energoatomizdat, Moscow, 1991.

[7] T.Lemczyk and M.Yovanovich, New Models and Methology for Predicting Thermal Contact Resistance, Heat-Transfer Engin., v.8, N2 (1987).

[8] Ju.Shlykov, E.Ganin, S.Tsarevsky, Contact Thermal Resistance, Energia, Moscow (1977).

[9] Z.Gorbis, A.Raffray, M.Abdou, Fusion Technology, v.19 (1991).

[10] M.Barbier, Induced Radioactivity, North-Holland Published Company, Amsterdam-London, 1969.

[11] I.Baishev, S.Kuchinin, N.Mokhov, Preprint IHEP 86-76, Protvino, 1986.